Nuclear Engineering and Technology 53 (2021) 3861–3878

Contents lists available at ScienceDirect

Nuclear Engineering and Technology

journal homepage: www.elsevier.com/locate/net

Original Article

Time-dependent simplified spherical harmonics formulations for a nuclear reactor system

A. Carreño [a], A. Vidal-Ferràndiz [b], D. Ginestar [b], G. Verdú [a, *]

[a] Instituto Universitario de Seguridad Industrial, Radiofísica y Medioambiental, Universitat Politècnica de València, Camino de Vera, s/n, 46022, València, Spain

[b] Instituto Universitario de Matemática Multidisciplinar, Universitat Politècnica de València, Camino de Vera, s/n, 46022, València, Spain

ARTICLE INFO

Article history:
Received 5 February 2021
Received in revised form
4 June 2021
Accepted 7 June 2021
Available online 22 June 2021

Keywords:
Implified spherical harmonic equations
Finite element method
Time-dependent neutron transport approximations

ABSTRACT

The steady-state simplified spherical harmonics equations (SP_N equations) are a higher order approximation to the neutron transport equations than the neutron diffusion equation that also have reasonable computational demands. This work extends these results for the analysis of transients by comparing of two formulations of time-dependent SP_N equations considering different treatments for the time derivatives of the field moments. The first is the full system of equations and the second is a diffusive approximation of these equations that neglects the time derivatives of the odd moments. The spatial discretization of these methodologies is made by using a high order finite element method. For the time discretization, a semi-implicit Euler method is used. Numerical results show that the diffusive formulation for the time-dependent simplified spherical harmonics equations does not present a relevant loss of accuracy while being more computationally efficient than the full system.

1. Introduction

The distribution of the neutrons inside a reactor core is modelled by means of the Boltzmann neutron transport equation. This integro-differential equation depends on four independent variables defined in a total of seven dimensions: three for the position, two for the direction of the neutrons, one for energy and one for time [1]. That makes obtaining the analytic solution (excluding some very simple problems) a very challenging problem. Therefore, two types of methodology are normally used to approximate this equation.

The first is to use stochastic methods such as the Monte-Carlo methodology, where discrete particle histories are tracked. Traditionally, these methods only allow steady-states computations. Recently, this kind of methods have been also used for dynamic computations [2–4].

The other alternative is to use deterministic methods that numerically solve approximations to the Boltzmann transport equation as a differential equations. Amongst the deterministic methods, there are many alternatives depending on the treatment of the continuous dependence of the independent variables.

For the energy dependence, the multigroup approximation is considered where the continuous energy is divided into several discrete energy groups. The approximation reduces the continuous equation into several monoenergetic equations that are coupled through the fission or the scattering terms. In this work, the spatial discretization is made by using a continuous Galerkin finite element method. This methodology has been applied to several approximations of the neutron transport equation giving very accurate results and using large nodes and a moderate number of degrees of freedom in the finite element expansion [5,6]. Moreover, this methodology can easily treat different kind of meshes in the discretization. This facilitates the analysis of reactors with any type of geometry (including hexagonal geometries or unstructured meshes for pin-level computations). This cannot be easily done with other discretizations such as finite difference methods or nodal methods as it is discussed in Refs. [7,8].

For the steady state computations, the time dependence is removed by forcing the criticality of the system. For that purpose, the λ-modes problem is used, which is obtained by dividing the fission term by a positive number λ. This problem is a generalized eigenvalue problem where the largest eigenvalue in magnitude corresponds to the k-effective of the nuclear system and the corresponding eigenfunction is associated with the neutronic flux distribution inside the core. Alternative problems can be defined,

* Corresponding author.
E-mail address: gverdu@iqn.upv.es (G. Verdú).

https://doi.org/10.1016/j.net.2021.06.010

but their computation is considerably more expensive [9]. Once the steady-state problem is obtained, different time schemes can be applied to discretize the time dependence of the equations. The most common method is to use a finite differences technique such as the implicit backward method [10,11]. Moreover, one can apply quasi-static methods that assume a decomposition of the flux as a product of two functions that are obtained by using two independent time scales [12,13]. Another possibility is to use modal methods that describe the flux as a linear combination of a set of dominant modes [14,15]. In this work, a stable semi-implicit scheme is used for the time discretization because first order schemes are a usual practice in the existing neutronic solvers. Future works will study more elaborated higher order schemes in time.

Finally, the angular dependence treatment usually classifies the approximations of the neutron transport equation. Over the years, the most used approximation is the neutron diffusion equation because, even though its use is limited by certain conditions, it gives accurate solutions with a relatively low computational cost. Nevertheless, to study new fuel designs and configurations with complex geometry more precise approximations of the neutron transport equations can be considered. The discrete ordinates equations (S_N equations) are obtained by using different quadrature sets for the angular discretization [16–18]. The spherical harmonics equations (P_N equations) are then obtained by expanding the angular variable in terms of spherical harmonics [19–21]. Moreover, one can apply the method of characteristics (MOC) that solves the neutron transport equation along a large enough set of characteristic lines generated by subdividing the solid angle domain into several discrete directions [22,23]. All these models for a realistic problem lead to large sets of equations that require petascale computing to be solved [24]. In order to reduce these high computational resources, a simplified formulation for the P_N equations was developed in Ref. [25] known as the simplified P_N equations or SP_N equations. This approximation is derived from the P_N equations for a one-dimensional geometry where the partial derivatives of the even moments are substituted by gradients and the partial derivatives of the odd moments are substituted by divergence operators. Even though this model is not convergent to the neutron transport equation, it has been shown to be an asymptotic correction to standard diffusion theory [26–28].

In the steady-state SP_N equations, odd moments are normally isolated and replaced again in the even moments equations, leading to a simplified formulation where only the even moments are part of the equations. Several works [29–31] have verified this approach. Another possibility is to consider the full set of equations (even and odd moments). Both strategies (theoretically equivalent) are used in this work for the time-dependent SP_N equations. In these equations, several approximations can be considered based on different assumptions related to the time derivative of the spherical harmonics moments. First, one can use the full SP_N equations where it is assumed that the time variation of all moments is different from zero (FSP_N equations). In a second approach, it is assumed that the odd moments are constant in time (DSP_N equations). This last consideration gives a simpler formulation than the first one because (as with in the steady-state problem) only the even moments appear in the equations and second order spatial derivatives appear leading to a generalized time-dependent diffusion equation. For the special case of $N = 1$, the FSP_1 and the DSP_1 equation (with isotropic scattering) are equivalent to the telegrapher's model and the neutron diffusion equation, respectively. Some works are devoted to comparing these two approximations showing a retardation in the time response as the relaxation time increases [32,33]. However, it is not clear that these results are maintained for $N > 1$ [34]. Finally, one can consider that only the time derivative of the scalar flux (first moment) is not equal to zero to obtain another time-dependent SP_N formulation [35].

The main objective of this work is to compare the full and the diffusive formulations of the time-dependent SP_N equations showing the differences between these two models for different type of transients. These transients display differences between the diffusion and higher approximations of the neutron transport equations. However, if the full P_N equations are used, they lead to very large problems which require super computers to be solve. This work also aims to verify the implementation of the proposed methodology using the finite element method for the spatial discretization and the semi-implicit difference method to approximate the time dependence of the SP_N equations. The results obtained are compared with the ones computed with other neutronic codes.

The rest of this paper is structured as follows. Section 2 presents the steady-state SP_N equations and the two treatments for the time-dependent SP_N equations considered here: the FSP_N and the DSP_N formulations. Section 3 briefly reviews the finite element method used for the spatial discretization of SP_N equations. Section 4 describes the semi-implicit time discretization scheme to integrate the time-dependent equations. Section 5 presents the analytical solutions of the time-dependent SP_1 and full SP_3 equations for a homogeneous slab. Section 6 contains the numerical results of this work for different benchmark problems. Finally, the paper ends with the main conclusions which were reached, (Section 7).

2. The time-dependent simplified spherical harmonics equations

The simplified spherical harmonics equations are normally obtained from the one-dimensional multigroup time-dependent spherical harmonics equations, P_N equations. These equations can be expressed in matrix form as [1].

$$\begin{aligned}
&\mathcal{V}\frac{\partial}{\partial t}\phi^0 + \frac{\partial}{\partial x}\phi^1 + \mathcal{S}^0\phi^0 = \mathcal{F}\phi^0 + \sum_{k=1}^{K}\mathcal{M}_k\mathcal{C}_k,\\
&\mathcal{V}\frac{\partial}{\partial t}\phi^n + \frac{\partial}{\partial x}\left(\frac{n}{2n+1}\phi^{n-1} + \frac{n+1}{2n+1}\phi^{n+1}\right) + \mathcal{S}^n\phi^n = 0\\
&n = 1,\ldots,N
\end{aligned} \tag{1}$$

where the equations for the delayed neutron precursor concentration are

$$\frac{\partial}{\partial t}\mathcal{C}_k = -\lambda_k^d\mathcal{C}_k + \mathcal{R}_k\phi^0 \qquad k = 1,\ldots,K. \tag{2}$$

In the previous equations, the spatial and time-dependent operators present are defined as

$$\phi^n = \left(\phi_1^n, \phi_2^n, \ldots, \phi_G^n\right)^T, \tag{3}$$

$$\mathcal{S}^n = \begin{pmatrix} \Sigma_{t1} - \Sigma_{s11}^n & -\Sigma_{s21}^n & \cdots & -\Sigma_{sG1}^n \\ -\Sigma_{s12}^n & \Sigma_{t2} - \Sigma_{s22}^n & \cdots & -\Sigma_{sG2}^n \\ \vdots & \vdots & \ddots & \vdots \\ -\Sigma_{s1G}^n & -\Sigma_{s2G}^n & \cdots & \Sigma_{tG} - \Sigma_{sGG}^n \end{pmatrix}, \tag{4}$$

$$\mathcal{F}=\begin{pmatrix} \chi_1^p\left(1-\beta^1\right)\nu_1\Sigma_{f1} & \chi_1^p\left(1-\beta^2\right)\nu_2\Sigma_{f2} & \dots & \chi_1^p\left(1-\beta^G\right)\nu_G\Sigma_{fG} \\ \chi_2^p\left(1-\beta^1\right)\nu_1\Sigma_{f1} & \chi_2^p\left(1-\beta^2\right)\nu_2\Sigma_{f2} & \dots & \chi_2^p\left(1-\beta^G\right)\nu_G\Sigma_{fG} \\ \vdots & \vdots & \ddots & \vdots \\ \chi_G^p\left(1-\beta^1\right)\nu_1\Sigma_{f1} & \chi_G^p\left(1-\beta^2\right)\nu_2\Sigma_{f2} & \dots & \chi_G^p\left(1-\beta^G\right)\nu_G\Sigma_{fG} \end{pmatrix}, \tag{5}$$

$$\mathcal{V}=\begin{pmatrix} 1/\nu_1 & 0 & \dots & 0 \\ 0 & 1/\nu_2 & \ddots & \vdots \\ \vdots & \ddots & \ddots & 0 \\ 0 & \dots & 0 & 1/\nu_G \end{pmatrix}, \qquad \mathcal{M}_k=\begin{pmatrix} \lambda_k^d\chi_1^{d,k} \\ \vdots \\ \lambda_k^d\chi_G^{d,k} \end{pmatrix}, \tag{6}$$

$$\mathcal{R}_k=\begin{pmatrix} \beta_k^1\nu_1\Sigma_{f1} & \cdots & \beta_k^G\nu_G\Sigma_{fG} \end{pmatrix} \tag{7}$$

The variable $\phi_g^n=\phi_g^n(x,t)$ denotes the nth-moment of the neutron flux. $\mathcal{C}_k$ denotes the delayed neutron precursor concentration. Subindex g ($g=1,\dots,G$) refers to the energy group and subindex k ($k=1,\dots,K$) refers to the precursor group. The total and the fission macroscopic cross-sections are denoted by Σ_t and Σ_f, respectively. The value of Σ_s^n is the nth-component of the scattering cross section in the spherical harmonics expansion. The value of ν is the mean number of neutrons produced by fission. The value of v denotes the neutron velocity. The spectrum of the prompt and the delayed neutrons are denoted by χ_g^p and $\chi_g^{d,k}$. The fraction of the delayed neutrons is β_k^g such that the total delayed neutron fraction $\beta^g=\sum_k^K\beta_k^g$. Finally, the neutron precursor delayed constants are represented by λ_k^d.

In the expressions above it is assumed that the scattering is isotropic, so the components of the scattering cross-sections are assumed to be equal to zero for moments equal or higher than 1. Moreover, the total cross-section, Σ_t, is approximated by the transport cross-section Σ_{tr}.

The absorption cross-section Σ_{ag}, which will appear later in the text, is equal to $\Sigma_t-\sum_{g'=1}^G\Sigma_{sgg'}$.

The P_N equations constitute a set of $N+1$ equations with $N+2$ unknowns. The most common option to solve this problem it to remove the term $d\phi^{N+1}/dx$ that appears in the N-th equation. Other solutions, known as closures, have also been studied in the literature [36].

From Equation (1), the steady-state problem can be obtained by dividing the fission term $\mathcal{F}$ by a positive number λ to force the criticality of the system. The steady-state P_N equations are

$$\begin{aligned} &\frac{d}{dx}\varphi^1+\mathcal{S}_{\text{stat}}^0\varphi^0=\frac{1}{\lambda}\bar{\mathcal{F}}\varphi^0, \\ &\frac{d}{dx}\left(\frac{n}{2n+1}\varphi^{n-1}+\frac{n+1}{2n+1}\varphi^{n+1}\right)+\mathcal{S}_{\text{stat}}^n\varphi^n=0,\ n=1,\dots,N. \end{aligned} \tag{8}$$

where $\varphi=\phi(x,0)$ is the steady-state flux, $\mathcal{S}_{\text{stat}}^0$ is the matrix given in Equation (4) at $t=0$, the new $\bar{\mathcal{F}}$ operator is defined as

$$\bar{\mathcal{F}}=\begin{pmatrix} \chi_1\nu_1\Sigma_{f1} & \chi_1\nu_2\Sigma_{f2} & \cdots & \chi_1\nu_G\Sigma_{fG} \\ \chi_2\nu_1\Sigma_{f1} & \chi_2\nu_2\Sigma_{f2} & \cdots & \chi_2\nu_G\Sigma_{fG} \\ \vdots & \vdots & \ddots & \vdots \\ \chi_G\nu_1\Sigma_{f1} & \chi_G\nu_2\Sigma_{f2} & \cdots & \chi_G\nu_G\Sigma_{fG} \end{pmatrix}, \tag{9}$$

and the value of χ_g is $\chi_g=\chi_g^p(1-\beta^g)+\sum_k^K\chi_g^{d,k}\beta_k^g$. The value for all magnitudes corresponds to the value of them at time $t=0$. The largest eigenvalue in magnitude corresponds to the k-effective of the system.

This system of differential equations must be completed with the boundary conditions of the reactor. In this work, we consider:

- Vacuum boundary conditions. We can use the Marshak's conditions that, given a boundary position x_0 and making use of the spherical harmonics expansion, can be written as

$$\int_{\mu_{in}}P_n(\mu)\sum_{n'=0}^N\frac{2n'+1}{2}\phi^{n'}(x_0)P_{n'}(\mu)\mathrm{d}\mu=0 \quad n=1,3,\dots,N \tag{10}$$

where P_n is the Legendre polynomial of degree n and μ is defined as $\mu\equiv cos(\theta)$ where θ is the angle between the x axis and the direction of the incident neutron velocity [1].

For instance, in the P_3 equations, if $\vec{n}$ is the normal direction at the boundary x_0, the Marshak's boundary conditions are:

$$\frac{1}{2}\phi^0+\frac{5}{8}\phi^2=\vec{n}\vec{\phi}^1,-\frac{1}{8}\phi^0+\frac{5}{8}\phi^2=\vec{n}\vec{\phi}^3. \tag{11}$$

- Reflective boundary conditions. In this case, the only conditions that make physical sense is forcing the odd moments are equal to zero [1],

$$\phi^n(x_0)=0\,,\quad n=1,3,\dots,N. \tag{12}$$

The angular flux moments of the steady-state problems obtained from the eigenvalue problem (8) are undetermined. Thus, a normalization criterion must be defined. The mean neutron power density production at time t is defined as

$$\bar{P}(t)=\frac{1}{V_t}\sum_{g=1}^G\int_\Omega\Sigma_{fg}\phi_g^0(\vec{r},t)dV, \tag{13}$$

where Ω is the reactor domain and V_t the total volume of the reactor. The normalization criterion is such that, at steady-state, the mean relative power production is equal to 1, i.e.

$$1=\bar{P}\,(0). \tag{14}$$

The extension of the steady-state P_N equations to be valid in multidimensional geometries to obtain the SP_N equations is done by substituting in the even n equations the derivative with respect to x by a divergence, and in the odd n equations the x derivative is changed by a gradient [25,28]. However, in the time-dependent case, several treatments for the time derivatives of the moments can be considered that yield different time-dependent SP_N formulations.

2.1. Full spherical harmonics equations (FSP$_N$ equations)

The full time-dependent multidimensional FSP$_N$ equations are

$$\begin{aligned}
&\mathcal{V}\frac{\partial}{\partial t}\phi^0 + \vec{\nabla}\cdot\vec{\phi}^{\,1} + \mathcal{S}^0\phi^0 = \mathcal{F}\phi^0 + \sum_{k=1}^{K}\mathcal{M}_k\mathcal{C}_k,\\
&\mathcal{V}\frac{\partial}{\partial t}\phi^n\vec{\nabla}\left(\frac{n}{2n+1}\phi^{n-1} + \frac{n+1}{2n+1}\phi^{n+1}\right) + \mathcal{S}^n\vec{\phi}^{\,n} = 0,\ n \text{ odd},\\
&\mathcal{V}\frac{\partial}{\partial t}\phi^n + \vec{\nabla}\cdot\left(\frac{n}{2n+1}\vec{\phi}^{\,n-1} + \frac{n+1}{2n+1}\vec{\phi}^{\,n+1}\right) + \mathcal{S}^n\phi^n = 0\ \ n>0,\ \text{even},
\end{aligned} \tag{15}$$

where $n = 1, \ldots, N$. The evolution of the delayed neutron precursor concentration is given by Equation (2). Note that this formulation yields to $(N + 1)\ (d + 1)/2$ scalar equations, where d is the dimension of the problem ($d = 1, 2, 3$).

The steady-state equations associated with the FSP$_N$ equations are

$$\begin{aligned}
&\vec{\nabla}\left(\frac{n}{2n+1}\varphi^{n-1} + \frac{n+1}{2n+1}\varphi^{n+1}\right) + \mathcal{S}^n\vec{\varphi}^{\,n} = 0, n \text{odd}.\\
&\vec{\nabla}\cdot\left(\frac{n}{2n+1}\vec{\varphi}^{\,n-1} + \frac{n+1}{2n+1}\vec{\varphi}^{\,n+1}\right) + \mathcal{S}^n\varphi^n = \delta_{n0}\frac{1}{\lambda}\mathcal{F}\varphi^0, n\text{even}.
\end{aligned} \tag{16}$$

2.2. Diffusive spherical harmonics equations (DSP$_N$ equations)

The idea of this approximation is to generalize the time-dependent neutron diffusion equation, that is equivalent to FSP$_1$ equations where the time derivative of the current ($\vec{\phi}^{\,1}$) is assumed to be equal to zero. In this way, for the different SP$_N$ equations we have

$$\frac{\partial}{\partial t}\vec{\phi}^{\,n} = 0, \qquad n \text{ odd}. \tag{17}$$

Equation (17) is then substituted into the FSP$_N$ equations (Equation (2.1)) to obtain, for $n = 1, \ldots, N$,

$$\mathcal{V}\frac{\partial}{\partial t}\phi^0 + \vec{\nabla}\cdot\vec{\phi}^{\,1} + \mathcal{S}^0\phi^0 = \mathcal{F}\phi^0 + \sum_{k=1}^{K}\mathcal{M}_k\mathcal{C}_k, \tag{18a}$$

$$\vec{\nabla}\left(\frac{n}{2n+1}\phi^{n-1} + \frac{n+1}{2n+1}\phi^{n+1}\right) + \mathcal{S}^n\vec{\phi}^{\,n} = 0 \qquad n \text{ odd}. \tag{18b}$$

$$\mathcal{V}\frac{\partial}{\partial t}\phi^n + \vec{\nabla}\cdot\left(\frac{n}{2n+1}\vec{\phi}^{\,n-1} + \frac{n+1}{2n+1}\vec{\phi}^{\,n+1}\right) \mathcal{S}^n\phi^n = 0 \quad n>0, \text{ even}. \tag{18c}$$

The equations for the delayed precursor concentrations are in Equation (2). System (18) has a particular advantage with respect to the full formulation. The odd moments of Equation (18b) can be isolated and substituted into Equations (18a) and (18c) to obtain the diffusive spherical harmonics equations (DSP$_N$ equations)

$$\begin{aligned}
&\mathcal{V}\frac{\partial}{\partial t}\phi^n - \vec{\nabla}\cdot\left(\frac{n\left(\mathcal{S}^{n-1}\right)^{-1}}{(2n+1)(2n-1)}\vec{\nabla}\left((n-1)\phi^{n-2} + n\phi^n\right)\right.\\
&\left. + \frac{(n+1)\left(\mathcal{S}^{n+1}\right)^{-1}}{(2n+1)(2n+3)}\vec{\nabla}\left((n+1)\phi^n + (n+2)\phi^{n+2}\right)\right) + \mathcal{S}^n\phi^n\\
&= \delta_{n0}\mathcal{F}\phi^n + \delta_{n0}\sum_{k=1}^{K}\mathcal{M}_k\mathcal{C}_k \qquad n = 0, 2, \ldots, N-1.
\end{aligned} \tag{19}$$

Note that, now, the number of scalar equations in this system is equal to $(N + 1)/2$. Also, the resulting system of the DSP$_N$ equations is a set of diffusion-like second order differential equations, which can be treated with similar methods to the ones used for the time-dependent neutron diffusion equation.

Using the linear change of variables proposed in Ref. [37] for the steady-state SP$_N$ equations, we define

$$U^m = (2m-1)\,\phi^{2m-2} + 2m\,\phi^{2m}, \qquad m = 1, 2, \ldots, M-1, \tag{20}$$

$$U^M = (2M-1)\,\phi^{2M-2}, \tag{21}$$

where $M = (N + 1)/2$ and U^m includes the group dependent diffusive pseudo-moments

$$U^m = \left(u_1^m, u_2^m, \ldots, u_G^m\right)^T, \tag{22}$$

to obtain the system

$$\mathbb{V}\frac{\partial}{\partial t}U - \vec{\nabla}\cdot(\mathbb{D}\vec{\nabla}U) + \mathbb{S}U = \mathbb{F}U + \mathbb{C}. \tag{23}$$

For instance, in the case of the P$_3$ equations, the change of variables is

$$U^1 = \phi^0 + 2\phi^2 \quad U^2 = 3\phi^2, \tag{24}$$

such that

$$U = \left(U^1, U^2\right)^T.$$

In Equation (23), the velocity matrix ($\mathbb{V}$), the effective diffusion matrix ($\mathbb{D}$), the absorption matrix ($\mathbb{S}$), the fission matrix ($\mathbb{F}$) and the precursors term ($\mathbb{C}$) are given by

$$\mathbb{D} = \begin{pmatrix} \frac{1}{3}\left(\mathcal{S}^1\right)^{-1} & 0 \\ 0 & \frac{1}{7}\left(\mathcal{S}^3\right)^{-1} \end{pmatrix}, \tag{25}$$

$$\mathbb{S}_{ij} = \sum_{m=1}^{2}\mathbf{c}_{ij}^{(\mathbf{m})}\mathcal{S}^m, \quad \mathbb{V}_{ij} = \sum_{m=1}^{2}\mathbf{c}_{ij}^{(\mathbf{m})}\mathcal{V}, \tag{26}$$

$$\mathbb{F}_{ij} = \mathbf{c}_{ij}^{(\mathbf{1})}\mathcal{F}, \quad \mathbb{C}_i = \mathbf{d}_i\sum_{p=1}^{K}\mathcal{M}_k\mathcal{C}_k, \tag{27}$$

where the coefficients matrix, $\mathbf{c}^{(m)}$ and vector $\mathbf{d}$ are

$$\mathbf{c}^{(\mathbf{1})} = \begin{pmatrix} 1 & -\frac{2}{3} \\ -\frac{2}{3} & \frac{4}{9} \end{pmatrix}, \quad \mathbf{c}^{(\mathbf{2})} = \begin{pmatrix} 0 & 0 \\ 0 & \frac{5}{9} \end{pmatrix}, \quad \mathbf{d} = \begin{pmatrix} 1 - \frac{2}{3} \end{pmatrix} \tag{28}$$

Following the same process and change of variables for the steady-state problem, we obtain the eigenvalue problem

$$-\vec{\nabla}(\mathbb{D}\,\vec{\nabla}U)+\mathbb{A}U=\frac{1}{\lambda}\bar{\mathbb{F}}U, \tag{29}$$

where in this case

$$\bar{\mathbb{F}}=\mathbf{c}_{ij}^{(1)}\bar{\mathbf{F}}\,. \tag{30}$$

Finally, the previous equations, the boundary conditions with this change of variables have the following forms [37].

The vacuum boundary conditions can be applied by forcing

$$-\vec{n}\,\mathbb{D}\vec{\nabla}U(x_0)=\mathbb{B}U(x_0), \tag{31}$$

where $\vec{n}$ is the normal direction to the boundary. For instance, the matrix $\mathbb{B}$ for the SP_3 case, is the result of the Kronecker product of matrix $\mathbf{b}$ by an $G\times G$ identity matrix as

$$\mathbb{B}=\mathbf{b}\otimes\mathbf{I}_{(G\times G)}\qquad \mathbf{b}=\begin{pmatrix}\frac{1}{2} & -\frac{1}{8}\\ -\frac{1}{8} & \frac{7}{24}\end{pmatrix} \tag{32}$$

The reflective boundary conditions are setting as

$$\vec{\nabla}U^m(x_0)=0,\qquad m=1,2,\ldots,(N+1)/2. \tag{33}$$

3. Spatial discretization: the finite element method

A high order finite element method is used for the spatial discretization of the previous differential equations. For simplicity, let us consider the steady-state problem and one energy group in the formulations to explain the finite element discretization method. The steady-state computation is the first step in any transient analysis. A similar process is applied for the spatial discretization of the time-dependent problems and problems with more energy groups.

We start with the steady-state SP_1 equation in the full version (with the odd and the even moments) assuming $\Sigma_s^1=0$ and denoting $\Sigma_s=\Sigma_s^0$ that is

$$\frac{1}{3}\vec{\nabla}\varphi^0+\Sigma_t\vec{\varphi}^1=0, \tag{34}$$

$$\vec{\nabla}\cdot\vec{\varphi}^1+(\Sigma_t-\Sigma_s)\varphi^0=\frac{1}{\lambda}\nu\Sigma_f\varphi^0. \tag{35}$$

In matrix form, the previous expression can be written as

$$\begin{pmatrix}(\Sigma_t-\Sigma_s) & \vec{\nabla}\\ \frac{1}{3}\vec{\nabla}\cdot & \Sigma_t\end{pmatrix}\begin{pmatrix}\varphi^0\\ \vec{\varphi}^1\end{pmatrix}=\frac{1}{\lambda}\begin{pmatrix}\nu\Sigma_f & 0\\ 0 & 0\end{pmatrix}\begin{pmatrix}\varphi^0\\ \vec{\varphi}^1\end{pmatrix} \tag{36}$$

First, we define the weak formulation of the problem by pre-multiplying it by a test function $(\psi^0,\vec{\psi}^1)$ and integrating over the reactor domain, Ω, to obtain

$$\begin{aligned}&\int_\Omega\left(\psi^0,\vec{\psi}^1\right)\begin{pmatrix}(\Sigma_t-\Sigma_s) & \vec{\nabla}\\ \frac{1}{3}\vec{\nabla}\cdot & \Sigma_t\end{pmatrix}\begin{pmatrix}\varphi^0\\ \vec{\varphi}^1\end{pmatrix}dV\\ &=\frac{1}{\lambda}\int_\Omega\left(\psi^0,\vec{\psi}^1\right)\begin{pmatrix}\nu\Sigma_f & 0\\ 0 & 0\end{pmatrix}\begin{pmatrix}\varphi^0\\ \vec{\varphi}^1\end{pmatrix}dV.\end{aligned} \tag{37}$$

Equation (37) is equivalent to

$$\begin{aligned}&\left(\psi^0,(\Sigma_t-\Sigma_s)\varphi^0\right)_\Omega+\left(\psi^0,\vec{\nabla}\cdot\vec{\varphi}^1\right)_\Omega\\ &+\frac{1}{3}\left(\vec{\psi}^1,\vec{\nabla}\varphi^0\right)_\Omega+(\vec{\psi}^1,\Sigma_t\vec{\varphi}^1)_\Omega\\ &=\frac{1}{\lambda}\left(\psi^0,\nu\Sigma_f\varphi^0\right)_\Omega,\end{aligned} \tag{38}$$

where $(a,b)_\Omega$ denotes the inner product $\int_\Omega a\cdot b\,dV$.

Now, if the Gauss identity is applied to the second term of Equation (3), we obtain

$$\left(\psi^0,\vec{\nabla}\cdot\vec{\varphi}^1\right)_\Omega=\vec{\nabla}\cdot\left(\psi^0,\vec{\varphi}^1\right)_\Omega-\left(\vec{\nabla}\psi^0,\vec{\varphi}^1\right)_\Omega, \tag{39}$$

and then, using the Divergence theorem on the second term of Equation (39)

$$\vec{\nabla}\cdot\left(\psi^0,\vec{\varphi}^1\right)_\Omega=\left(\psi^0,\vec{n}\vec{\varphi}^1\right)_{\partial\Omega}, \tag{40}$$

Equation (38) is transformed into

$$\begin{aligned}&\left(\psi^0,(\Sigma_t-\Sigma_s)\varphi^0\right)_\Omega+\left(\psi^0,\vec{n}\vec{\varphi}^1\right)_{\partial\Omega}-\left(\vec{\nabla}\psi^0,\vec{\varphi}^1\right)_\Omega\\ &+\frac{1}{3}\left(\vec{\psi}^1,\vec{\nabla}\varphi^0\right)_\Omega(\vec{\psi}^1,\Sigma_t\vec{\varphi}^1)_\Omega=\frac{1}{\lambda}\left(\psi^0,\nu\Sigma_f\varphi^0\right)_\Omega,\end{aligned} \tag{41}$$

where $\partial\Omega$ is the boundary of the domain and $(a,b)_{\partial\Omega}=\int_{\partial\Omega}a\cdot b\,dS$.

The last step is to divide the domain Ω into cells or subdomains Ω_c such that $\Omega=\cup_{c=1,\ldots,N_c}\Omega_c$ where it is supposed that the cross-sections, obtained by a previous spatial homogenization strategy, are constant. Likewise, $\partial\Omega_c$ is the corresponding subdomain surface which is part of the boundary $\partial\Omega$. Thus, Equation (3) is equivalent to

$$\begin{aligned}&\sum_{c=1}^{N_c}(\Sigma_t^c-\Sigma_s^c)\left(\psi^0,\varphi^0\right)_{\Omega_c}+\sum_{c=1}^{N_c}\left(\psi^0,\vec{n}\vec{\varphi}^1\right)_{\partial\Omega_c}-\sum_{c=1}^{N_c}\left(\vec{\nabla}\psi^0,\vec{\varphi}^1\right)_{\Omega_c}\\ &+\sum_{c=1}^{N_c}\frac{1}{3}\left(\vec{\psi}^1,\vec{\nabla}\varphi^0\right)_{\Omega_c}+\sum_{c=1}^{N_c}\Sigma_t^c(\vec{\psi}^1,\vec{\varphi}^1)_{\Omega_c}=\frac{1}{\lambda}\sum_{c=1}^{N_c}\nu\Sigma_f^c\left(\psi^0,\varphi^0\right)_{\Omega_c}.\end{aligned} \tag{42}$$

To solve the integrals over the subdomains, Ω_c, the function φ^0 and the components of $\vec{\varphi}^1=(\varphi_x^1,\varphi_y^1,\varphi_z^1)$ are approximated as sum of shape functions, $\mathcal{N}_a$, multiplied by the unknown expansion coefficients as

$$\varphi^0 \approx \sum_{a=0}^{N_{\text{dofs}}} \mathcal{N}_a \widetilde{\varphi}_a^0 \qquad \vec{\varphi}^1 \approx \sum_{a=0}^{N_{\text{dofs}}} \mathcal{N}_a \widetilde{\vec{\varphi}}_a^1 , \tag{43}$$

where N_{dofs} is the total number of degrees of freedom.

A continuous Galerkin approximation is used such that the test functions space is the same as the space defined by the basis of shape functions. The shape functions are taken as Lagrange polynomials [38].

If one uses the above assumptions in Equation (3), the following algebraic eigenvalue problem is obtained

$$A\widetilde{\varphi} = \frac{1}{\lambda} B\widetilde{\varphi}, \tag{44}$$

where

$$A = \begin{pmatrix} A_{11} & A_{12} \\ A_{21} & A_{22} \end{pmatrix}, \qquad B = \begin{pmatrix} B_{11} & 0 \\ 0 & 0 \end{pmatrix}, \qquad \widetilde{\varphi} = \begin{pmatrix} \widetilde{\varphi}^0 \\ \widetilde{\vec{\varphi}}^1 \end{pmatrix}, \tag{45}$$

and the matrices elements (a, b) are taken as

$$A_{11(ab)} = \sum_{c=1}^{N_c} (\Sigma_t^c - \Sigma_s^c)(\mathcal{N}_a, \mathcal{N}_b)_{\Omega_c}, \; A_{21(ab)} = \frac{1}{3} \sum_{c=1}^{N_c} \left(\vec{\mathcal{M}}_a, \vec{\nabla} \mathcal{N}_b \right)_{\Omega_c},$$

$$A_{12(ab)} = \sum_{c=1}^{N_c} \left(\left(\mathcal{N}_a, \vec{n} \vec{\mathcal{M}}_b \right)_{\partial\Omega_c} - \left(\vec{\nabla} \mathcal{N}_a, \vec{\mathcal{M}}_b \right)_{\Omega_c} \right),$$

$$A_{22(ab)} = \sum_{c=1}^{N_c} \Sigma_t^c \left(\vec{\mathcal{M}}_a, \vec{\mathcal{M}}_b \right)_{\Omega_c}, \; B_{11(ab)} = \sum_{c=1}^{N_c} \nu\Sigma_f^c (\mathcal{N}_a, \mathcal{N}_b)_{\Omega_c},$$

where $\vec{\mathcal{M}}_a = (\mathcal{N}_a, \mathcal{N}_a, \mathcal{N}_a)$.

In the expressions above surface integrals over the boundaries, $\partial\Omega_c$, appear. They will depend on the boundary conditions. The value of $\vec{n}\vec{\mathcal{M}}_b$ is substituted by the first term of expression (32) if vacuum boundary conditions are used or by zero if reflective boundary conditions are employed.

These integrals only are different from zero if shape functions $\mathcal{N}_a$ and $\mathcal{N}_b$ collide inside the same cell. Therefore, sparse matrices are obtained. For a general problem with G energy groups, N moments and dimension d the size of the matrices is $N_t = N_{\text{dofs}} G(d+1)(N+1)/2$.

To solve the algebraic generalized eigenvalue problem (44), the generalized Davidson method, implemented by the open source library SLEPc, is used [39]. This eigenvalue solver updates the eigenvector of a matrix by solving a linear system with an approximation of this matrix known as preconditioner [40]. Usually, this approximation behaves better than the original matrix. In this case, the ILU(0) factorization is taken from the library PETSc as preconditioner [41]. Note that the matrices obtained have a block structure. However, the nature of this formulation means that block methods proposed in previous works by the authors [31], do not converge as fast as before. Therefore, the eigenvalue solver is applied directly to the entire matrices without taking into account their block structure.

Now, the finite element process for the diffusive steady-state SP_1 equations is shown. For that, we use the one energy group equation

$$\left(-\vec{\nabla} \frac{1}{3} \Sigma_t \vec{\nabla} + (\Sigma_t - \Sigma_s) \right) \psi = \frac{1}{\lambda} \nu\Sigma_f \psi. \tag{46}$$

The weak formulation in this case is

$$\left(\psi, \left(-\vec{\nabla} \left(\frac{1}{3} \Sigma_t \vec{\nabla} \right) + (\Sigma_t - \Sigma_s) \right) \varphi \right)_\Omega = \frac{1}{\lambda} \left(\psi, \nu\Sigma_f \varphi \right)_\Omega, \tag{47}$$

where ψ is a test function.

As in the previous case, the reactor domain Ω is decomposed as a sum of subdomains Ω_c and the solution φ is approximated in each node as a sum of shape functions $\mathcal{N}_a$ as

$$\varphi \approx \sum_{a=1}^{N_{dofs}} \mathcal{N}_a \widetilde{\varphi}_a. \tag{48}$$

To apply this finite element method, the Galerkin approximation and Lagrange polynomials are also used.

Introducing the assumptions into the weak formulation (47) and using the Gauss Divergence theorem yields a generalized algebraic eigenvalue problem

$$A\widetilde{\varphi} = \frac{1}{\lambda} B\widetilde{\varphi}, \tag{49}$$

where the matrix elements are now given by

$$A_{ab} = \sum_{c=1}^{N_c} \left(\frac{1}{3} \Sigma_t^c (\vec{\nabla} \mathcal{N}_a, \vec{\nabla} \mathcal{N}_b)_{\Omega_c} - \frac{1}{3} \Sigma_t^c \left(\mathcal{N}_a, \vec{n} \vec{\nabla} \mathcal{N}_b \right)_{\partial\Omega_c} + (\Sigma_t^c - \Sigma_s^c)(\mathcal{N}_a, \mathcal{N}_b)_{\Omega_c} \right),$$

$$B_{ab} = \sum_{c=1}^{N_c} \nu\Sigma_f^c (\mathcal{N}_a, \mathcal{N}_b), \tag{50}$$

where the boundary conditions are used to compute the boundary integral in the above expressions. See more details in Ref. [5].

For a general problem, the size of the matrices obtained with this diffusive formulation is $N_t = (N+1)GN_{\text{dofs}}/2$, that is $d+1$ times smaller than the size of the full formulation, where d is the dimension of the problem.

In this case, to solve the generalized eigenvalue problem (49), the block inverse-free preconditioned Arnordi method (BIFPAM) is used [31]. This method updates the successive eigenvectors by computing the Krylov subspace associated to the residual matrix $(B - \lambda A)$. Its convergence can be accelerated with a preconditioner of this residual matrix. In particular, it uses the block Gauss-Seidel preconditioner that takes advantage of the block structure that appears if the number of moments and energy groups are greater than 1.

The finite element method for the two formulations has been implemented using the open source finite elements library Deal. II [42]. For time-dependent problems, similar processes can be applied in each case that lead to semi-discrete problems whose time discretization will be described in next Section.

4. Time discretization: the semi-implicit method

Independently of the chosen formulation for the SP_N equations, the spatial discretization of the time-dependent problems yields to a semi-discrete problem of the form

$$V \frac{d}{dt} \Phi + T\Phi = F\Phi + \sum_{p=1}^{N_p} M_p C_p, \tag{51}$$

where V, T and F are the discretized operator of the velocity, the production and the fission, respectively. The form of these operators will depend on the formulation. The vector Φ contains the

discrete version of the moments, $\widetilde{\phi}$ for FSP_N or $\widetilde{U}$ for DSP_N equations. The vector C_k is the discretization of delayed neutron precursor concentration $\mathcal{C}_k$. The matrix M_k is the discretized operator of $\mathcal{M}_k$.

Analogously, the equation for the concentration of delayed precursors is

$$\frac{d}{dt}PC_k = -L_k C_k + R_k\widetilde{\phi}^0, \tag{52}$$

where L_k and R_k are the discretized operator of $\mathcal{L}_p = \lambda_k^d$ and $\mathcal{R}_k$, respectively. The matrix P denotes the mass matrix that is different from the identity matrix because the basis of the FEM (Lagrange polynomials) is not orthonormal.

Usually, for nuclear systems, the time-dependent semi-discrete ordinary differential equation (4) are stiff, thus, it is suitable to use implicit methods for its time discretization. Basically, this system is composed of two sets of equations: one set for the moments and another set for the concentration of delayed precursors, that are coupled. The complete system can be assembled (obtaining only one matrix equation) to design a full implicit scheme. However, this treatment is computationally very expensive. In this work, the alternative is to consider each set of equations independently and to use a semi-implicit scheme (prompt implicit) because this kind of scheme is cheaper and provides accurate results for the range of selected time-steps. Other alternative can be splitting methods [43].

The time interval $[0, T]$ is divided into several subintervals $[t_h, t_{h+1}]$ where $\Delta t_h = t_{h+1} - t_h$. First, the moments at $t = t_{h+1}$ are approximated by applying a backward difference of first order for the partial time derivative. The rest of terms are then substituted by its value at time t_{h+1} except the concentration of precursors term. For this case, we substitute the matrix by its value at time t_h. Thus, the vector of moments at time t_{h+1} can be approximated by solving the linear system

$$\left(\frac{1}{\Delta t_h}V^{h+1} + T^{h+1} - F^{h+1}\right)\Phi^{h+1} = \frac{1}{\Delta t_h}V^h\Phi^h + \sum_{k=1}^{K} M_k^{h+1}C_k^h, \tag{53}$$

where the superindex h denotes the value of matrices and vectors at time t_h.

This linear system is solved with the GMRES method provided by the PETSc library [41]. Two different preconditioners are used to solve the linear system. For the FSP_N equations, the ILU(0) factorization with a Cuthill McKee reordering is used from PETSc library. For the DSP_N equations, a block Gauss-Seidel preconditioner is used. The inverses in the Gauss-Seidel method are approximated by solving linear systems with the conjugate gradient method, the ILU preconditioner and a residual error of 10^{-5} are used in this case. This last strategy permits a partial matrix-free implementation that avoids the full assembly of the matrices at each time-step. See more details in Ref. [31].

Then, the concentration of delayed precursors equation is integrated. For that, we use a one-step implicit scheme where the time derivative is approximated by a backward difference of first order. The rest of the terms are approximated by their values at time t_{h+1}. In this way, the concentration of precursors can be approximated by solving the linear system

$$\left(\frac{1}{\Delta t_h}P + L_k^h\right)C^{h+1} = \frac{1}{\Delta t_h}PC^h + R_k^h\widetilde{\phi}^{0,h+1}. \tag{54}$$

This last system is solved with the GMRES method and the ILU(0) preconditioner provided by the PETSc library.

5. Analytical solutions of the FSP_1, DSP_1 and FSP_3 equations for a homogeneous slab

To compare theoretically both approximations, a homogeneous slab is defined since an analytical solution can be obtained in this case. One energy group is used in the approximations and neutron precursors are no considered.

Let us consider a homogeneous slab of length L with vacuum conditions on its boundaries where an instantaneous constant perturbation in the fission term $\nu\Sigma_f$ equal to $\Delta\Sigma_f$ is applied to obtain a transient.

5.1. FSP_1 equations

The one energy group FSP_1 equations for the homogeneous slab are of form

$$\begin{cases} \dfrac{1}{\nu}\dfrac{\partial}{\partial t}\phi^1(x,t) + \dfrac{1}{3}\dfrac{\partial}{\partial x}\phi^0(x,t) + \Sigma_t\phi^1(x,t) = 0 \\ \dfrac{1}{\nu}\dfrac{\partial}{\partial t}\phi^0(x,t) + \dfrac{\partial}{\partial x}\phi^1(x,t) + \Sigma_a\phi^0(x,t) = \left(\nu\Sigma_f^0 + \Delta\Sigma_f(t)\right)\phi^0(x,t) \\ \dfrac{1}{2}\phi^0(0,t) = -\phi^1(0,t), \quad \dfrac{1}{2}\phi^0(L,t) = \phi^1(L,t) \\ \phi^0(x,0) = \varphi^0(x) \quad \phi^1(x,0) = \varphi^1(x), \quad \Delta\Sigma_f(0) = 0. \end{cases} \tag{55}$$

The solution of the steady-state problem is [44].

$$\varphi^0(x) = c\left(\sin\left(\tau\frac{x}{L}\right) + \frac{2\tau}{3\Sigma_t L}\cos\left(\tau\frac{x}{L}\right)\right), \tag{56}$$

$$\varphi^1(x) = \frac{c}{3\Sigma_t}\left(\frac{\tau}{L}\cos\left(\tau\frac{x}{L}\right) - \frac{2\tau^2}{3\Sigma_t L^2}\sin\left(\tau\frac{x}{L}\right)\right), \tag{57}$$

where τ is a positive solution of the nonlinear equation

$$f_1(\tau) = \left(1 - \frac{4}{9(\Sigma_t L)^2}\tau^2\sin(\tau) + \frac{4}{3\Sigma_t L}\tau\cos(\tau)\right) = 0,$$

and the constant c is chosen from a normalization of the moments (Equation (14)).

The k-effective of the system is given by

$$k_{\text{eff}} = \frac{\nu\Sigma_f}{\Sigma_a + \tau^2\Big/\left(3\Sigma_t L^2\right)}.$$

In the time computation, the reactor at initial state is considered critical by dividing the Σ_f by k_{eff}. This satisfies

$$\nu\Sigma_f = \Sigma_a + \frac{\tau^2}{3L^2\Sigma_t}. \tag{58}$$

To solve the time-dependent problem, we assume

$$\phi^0(x,t) = n_0(t)\varphi^0(x), \qquad \phi^1(x,t) = n_1(t)\varphi^1(x).$$

This can be assumed because the transient is defined from a global perturbation in the reactor.

Equation (55) is then transformed into

$$\begin{aligned}&\frac{1}{v}\varphi^1\frac{d}{dt}n_1+\frac{1}{3}n_0\frac{d}{dx}\varphi_0+\Sigma_t n_1\varphi^1=0,\\&\frac{1}{v}\varphi^0\frac{d}{dt}n_0+n_1\frac{d}{dx}\varphi^1+\Sigma_a n_0\varphi^0=\left(\nu\Sigma_f+\Delta\Sigma_f\right)n_0\varphi^0,\end{aligned}\tag{59}$$

Now, the steady-state relations

$$\varphi^1=-\frac{1}{3\Sigma_t}\frac{d}{dx}\varphi^0,\qquad \frac{d^2}{dx^2}\varphi^0=-\frac{\tau^2}{L^2}\varphi^0,\tag{60}$$

are substituted into Equation (59) to obtain

$$\begin{aligned}&-\frac{1}{v}\frac{1}{3\Sigma_t}\frac{d}{dx}\varphi^0\frac{d}{dt}n_1+\frac{1}{3}n_0\frac{d}{dx}\varphi_0-\Sigma_t n_1\frac{1}{3\Sigma_t}\frac{d}{dx}\varphi^0=0,\\&\frac{1}{v}\varphi^0\frac{d}{dt}n_0+n_1\frac{1}{3\Sigma_t}\frac{\tau^2}{L^2}\varphi^0+\Sigma_a n_0\varphi^0=\left(\nu\Sigma_f+\Delta\Sigma_f\right)n_0\varphi^0,\end{aligned}\tag{61}$$

that is equivalent (if $\varphi^0\neq 0$ and $\frac{d}{dx}\varphi^0\neq 0$) to

$$\frac{1}{v}\frac{1}{3\Sigma_t}\frac{d}{dt}n_1-\frac{1}{3}n_0+\frac{1}{3}n_1=0\tag{62}$$

$$\frac{1}{v}\frac{d}{dt}n_0+\frac{1}{3\Sigma_t}\frac{\tau^2}{L^2}n_1+\Sigma_a n_0=\left(\nu\Sigma_f+\Delta\Sigma_f(t)\right)n_0\tag{63}$$

Then, isolating the term n_1 from Equation (63) and substituting into Equation (62) yields the second order differential equation

$$\frac{d^2}{dt^2}n_0-v\left(\frac{\tau^2}{L^2 3\Sigma_t}+\Delta\Sigma_f-\Sigma_t\right)\frac{d}{dt}n_0-v^2\Sigma_t\Delta\Sigma_f n_0=0,\tag{64}$$

whose solution is

$$n_0(t)=C_1e^{t\frac{v}{2}r_+}+C_2e^{t\frac{v}{2}r_-},\tag{65}$$

where $r_\pm=(\tau^2/(3L^2\Sigma_t)+\Delta\Sigma_f-\Sigma_t)\pm\sqrt{(\tau^2/(3L^2\Sigma_t)+\Delta\Sigma_f-\Sigma_t)^2+4\Sigma_t\Delta\Sigma_f}$, and C_1, C_2 are constants that are obtained by imposing $n_0(0)=1$ and $n_1(0)=1$.

Note that Equation (64) is similar to the telegrapher's equation. This is a differential equation of second order for the time variable that is the result of removing the neutronic current equation in the P_1 approximation and assuming that the Fick's law is no longer valid for a transient [45].

5.2. DSP_1 equations

Starting with the same conditions as in the previous case, the one energy group DSP_1 problem is of the form

$$\begin{cases}\frac{1}{v}\frac{\partial}{\partial t}\phi^0(x,t)-\frac{1}{3\Sigma_t}\frac{\partial^2}{\partial x^2}\phi^0(x,t)+\Sigma_a\phi^0(x,t)=\left(\nu\Sigma_f^0+\Delta\Sigma_f(t)\right)\phi^0(x,t)\\ \frac{1}{2}\phi^0(0,t)=\frac{1}{3\Sigma_t}\frac{\partial}{\partial x}\phi^0(0,t),\ \ \frac{1}{2}\phi^0(x_L,t)=-\frac{1}{3\Sigma_t}\frac{\partial}{\partial x}\phi^0(x_L,t),\\ \phi^0(L,t)=0,\ \phi^0(x,0)=\varphi,\ \Delta\Sigma_f(0)=0,\end{cases}\tag{66}$$

The solution to the steady-state problem associated is the same as in the previous formulation (Equation (56)).

To compute the solution of the time-dependent problem, it is assumed that

$$\phi^0(x,t)=n(t)\varphi_0(x).\tag{67}$$

This can be assumed because the transient is defined from a global perturbation in the reactor.

Thus Equation (66) can be expressed as

$$\frac{1}{v}\varphi_0\frac{d}{dt}n-\frac{1}{3\Sigma_t}n\frac{d^2}{dx^2}\varphi_0+\Sigma_a n\varphi_0=\left(\nu\Sigma_f^0+\Delta\Sigma_f\right)n\varphi_0.\tag{68}$$

Making use of the second steady-state identity (60), Equation (58) and supposing that $\varphi^0\neq 0$, Equation (68) is equivalent to

$$\frac{d}{dt}n=\nu\Delta\Sigma_f n,\tag{69}$$

which is a first order equation whose solution (with $n(0)=1$) is

$$n(t)=e^{\nu\Delta\Sigma_f t}.\tag{70}$$

5.3. Comparison between the FSP_1 and DSP_1 approximations

From the analytical solutions for both approximations, it can be concluded (under some assumptions) that the difference between these approximations will be dependent on the value of

$$\alpha=\frac{\tau^2}{3L^2\Sigma_t},\tag{71}$$

such that the $FSPN_1$ nears to $DSPN_1$ as α goes to 0.

To check this statement, the time components of the scalar moments, $n_0(t)$ and $n(t)$, are compared. We start with the solution of the FSP_1 equations. If we assume that $\alpha\approxeq 0$, the roots of the characteristic polynomial associated with the differential equation (64) are equal to

$$r_+^*=2\Delta\Sigma_f\quad r_-^*=-2\Sigma_t,\tag{72}$$

thus, the new solution for the FSP_1 equations would have the form

$$n_0^*(t)=C_1^*e^{\nu\Delta\Sigma_f}+C_2^*e^{-\nu\Sigma_t}.\tag{73}$$

As the value of the velocity v is usually greater than 10^4 for realistic reactor problems, the second term is very close to zero. Therefore, it is obtained that $n_0^*(t)\approxeq n(t)$.

Numerical results will show this statement by changing the length of the slab L.

In [32,33] the authors got a similar result using the relaxation time defined as $1/(\Sigma_t v)$ for a ramp insertion and a sinusoidal perturbation in the reactivity. Values for the relaxation time close to zero reduce the differences between these approximations.

5.4. Point kinetics solution for the FP_3 equations

Given a slab reactor with the same conditions as the previous cases, the one energy group time-dependent FSP_3 problem can be expressed as

$$\begin{aligned}&\frac{1}{v}\frac{\partial}{\partial t}\phi^0+\frac{\partial}{\partial x}\phi^1+\Sigma_a\phi^0=\left(\nu\Sigma_f+\Delta f\right)\phi^0,\\&\frac{3}{v}\frac{\partial}{\partial t}\phi^1+2\frac{\partial}{\partial x}\phi^2+\frac{\partial}{\partial x}\phi^0+3\Sigma_t\phi^1=0,\\&\frac{5}{v}\frac{\partial}{\partial t}\phi^2+3\frac{\partial}{\partial x}\phi^3+\frac{\partial}{\partial x}\phi^1+5\Sigma_t\phi^2=0,\\&\frac{7}{v}\frac{\partial}{\partial t}\phi^3+3\frac{\partial}{\partial x}\phi^2+7\Sigma_t\phi^3=0.\end{aligned}\tag{74}$$

If a point kinetics approximation is assumed, then

$$\phi^n(x,t) = n(t)\varphi_n(x), \quad n = 0, \ldots, 3,$$

where $\varphi_n(x)$ are the solution of the steady-state equations associated. These solutions can be found in Ref. [44].

From this consideration, the system of equation (5.4) is equivalent to

$$\begin{aligned}
&\frac{1}{v}\frac{d}{dt}n\varphi_0 + n\left(\frac{\partial}{\partial x}\varphi_1 + \Sigma_a\varphi_0 - \nu\Sigma_f\varphi_0\right) - \Delta f n\varphi_0,\\
&\frac{3}{v}\frac{d}{dt}n\varphi_1 + n\left(2\frac{\partial}{\partial x}\varphi_2 + \frac{\partial}{\partial x}\varphi_0 + 3\Sigma_t\varphi_1\right) = 0,\\
&\frac{5}{v}\frac{d}{dt}n\varphi_2 + n\left(3\frac{\partial}{\partial x}\varphi_3 + \frac{\partial}{\partial x}\varphi_1 + 5\Sigma_t\varphi_2\right) = 0,\\
&\frac{7}{v}\frac{d}{dt}n\varphi_3 + n\left(3\frac{\partial}{\partial x}\varphi_2 + 7\Sigma_t\varphi_3\right) = 0.
\end{aligned} \tag{75}$$

As $\varphi_n(x)$ satisfy the steady-state equations, system (5.4) is equivalent to

$$\frac{dn}{dt}\begin{pmatrix} \frac{1}{v}\varphi_0 \\ \frac{3}{v}\varphi_0 \\ \frac{5}{v}\varphi_0 \\ \frac{7}{v}\varphi_0 \end{pmatrix} - n\begin{pmatrix} \Delta\Sigma_f\varphi_0 \\ 0 \\ 0 \\ 0 \end{pmatrix} = 0 \tag{76}$$

Finally, if Equation (76) is collapsed by the left premultiplying by the transpose of the spatial vectors, the value of $n(t)$ can be computed by solving the ordinary differential equation with the initial condition $n(0) = 1$,

$$\begin{aligned}
&\left(\varphi^{0,T}, \varphi^{1,T}, \varphi^{2,T}, \varphi^{3,T}\right)\cdot\begin{pmatrix} \frac{1}{v}\varphi_0 \\ \frac{3}{v}\varphi_0 \\ \frac{5}{v}\varphi_0 \\ \frac{7}{v}\varphi_0 \end{pmatrix}\frac{dn}{dt}\\
&-\left(\varphi^{0,T}, \varphi^{1,T}, \varphi^{2,T}, \varphi^{3,T}\right)\cdot\begin{pmatrix} \Delta\Sigma_f\varphi_0 \\ 0 \\ 0 \\ 0 \end{pmatrix} n = 0.
\end{aligned} \tag{77}$$

6. Numerical results

This Section tests the performance of the FSP_N and the DSP_N equations for a different type of transients. First, a homogeneous slab is used to validate the implementation of the methods. This problem will also be used to study the convergence of the proposed semi-implicit scheme for the time-discretization. Furthermore, two transients with the TWIGL reactor are analysed to compare the results with other types of codes and neutron approximations. Finally, other transients for the C5G2 MOX reactor are defined to analyse the methodology in a more realistic reactor where the neutron diffusion equation is not very accurate.

For the finite element method, polynomials of degree 3 are used. This value has been shown to obtain accurate enough results for usual reactor calculations [5]. The dominant eigenvalue is computed with a residual tolerance of 10^{-12}.

For the semi-implicit time method, tolerances of 10^{-13} in the GMRES method are required to solve the associated linear systems. The time-steps for the semi-implicit scheme are considered constant along the transient and its size will depend on the transient analysed.

The time-dependent formulations for the spherical harmonics equation, FSP_N and DSP_N, have been implemented in C++ language. They have been incorporated to the open source code `FEMFFUSION` as an extension of the code. This neutronic code solves the neutron diffusion equation and the steady-state SP_N equations by using a high order finite element method. The full description and the source code of `FEMFFUSION` is available in Ref. [46].

All calculations have been carried out sequentially on an Intel® Core™i7-4790 3.60 GHz with 32 Gb of RAM running on Ubuntu GNU/Linux 18.04 LTS.

6.1. A homogeneous slab benchmark

We consider a homogeneous slab to define a simple transient whose solution for the FSP_1 and DSP_1 equations can be obtained analytically as has been shown in Section 5. Moreover, the analytical solution of the FSP_3 equations can be approximated with the solution of the point kinetics formulation (Section 5.4). Table 1 contains the cross-section data for this problem. Delayed precursors are not considered. For the spatial discretization, 8 cells of size 1.25 cm are used, and the boundary conditions are vacuum boundary conditions at both sides of the slab. The transient is defined from an instantaneous constant perturbation in the fission cross-section, $\Delta\Sigma_f = 10^{-4}$ cm^{-1}.

The multiplicative factor computed for the numerical steady-state SP_1 equations (with both formulations) is 0.994017 and the analytical value is 0.9940168. The k-effective for the SP_3 equations is 0.999999 and the analytical value is 1.000000.

First, we study the convergence of the semi-implicit time scheme. The results are given for the DSP_1 equations, but analogous conclusions are deduced for the rest of equations. Table 2 displays the relative local error (LE) between the analytical solution and the numerical solution computed as

$$\mathrm{LE} = \frac{\left\|\phi^0_{num} - \phi^0_{ana}\right\|}{\left\|\phi^0_{ana}\right\|}\cdot 100. \tag{78}$$

The relative local error decreases as the time-step Δt becomes smaller. Values of time-step (Δt) equal to 0.01 s and smaller provide

Table 1
Cross-section data of the homogeneous slab.

v (cm/s)	Σ_t (cm^{-1})	Σ_a (cm^{-1})	Σ_f (cm^{-1})	ν
10^4	1.0	0.1	0.062464	2.0

Table 2
Evolution in the relative local error (LE) in % between the numerical and the analytical scalar moments of the DSP_1 equations with different time-steps (Δt) for the semi-implicit time scheme.

$\Delta t(s)$	$t = 0.0$ s	$t = 0.1$ s	$t = 0.25$ s	$t = 0.50$	$t = 1.00$ s
0.1	3.3e-04	6.1e-01	–	2.80	5.59
0.01	3.3e-04	1.3e-01	2.0e-01	3.3e-01	5.8e-01
0.001	3.3e-04	8.5e-02	9.3e-02	1.1e-01	1.3e-01
0.0001	3.3e-04	8.0e-02	8.1e-02	8.3e-02	8.7e-02

Table 3
Evolution of the mean relative power (P) and relative local error (LE) in % obtained with the numerical and analytical FSP_N and the DSP_N equations ($N = 1, 3$) taking $\Delta t = 0.001$ s for the homogeneous reactor.

	Sol.	$t = 0.0$ s	$t = 0.1$ s	$t = 0.25$ s	$t = 0.50$ s	$t = 0.75$ s	$t = 1.00$ s
$\bar{P}^{FSP_1}$	Num.	1.0	1.10835	1.29174	1.66727	2.15197	2.77758
$\bar{P}^{FSP_1}$	Ana.	1.0	1.10808	1.29251	1.67058	2.15926	2.79087
LE^{FSP_1}		3.3e-04	2.4e-02	5.8e-02	1.9e-01	3.3e-01	4.7e-01
$\bar{P}^{DSP_1}$	Num.	1.0	1.10611	1.28521	1.65046	2.11951	2.72064
$\bar{P}^{DSP_1}$	Ana.	1.0	1.10517	1.28403	1.64872	2.11700	2.71828
LE^{DSP_1}		3.3e-04	8.5e-02	9.3e-02	1.1e-01	1.2e-01	1.3e-01
$\bar{P}^{FSP_3}$	Num.	1.0	1.10818	1.29123	1.66595	2.14941	2.77317
$\bar{P}^{FSP_3}$	Ana.	1.0	1.11371	1.30898	1.71342	2.24282	2.93580
LE^{FSP_3}		8.2e-01	8.2e-01	8.2e-01	8.2e-01	8.2e-01	8.2e-01
$\bar{P}^{DSP_3}$	Num.	1.0	1.10601	1.28492	1.64971	2.11806	2.71937

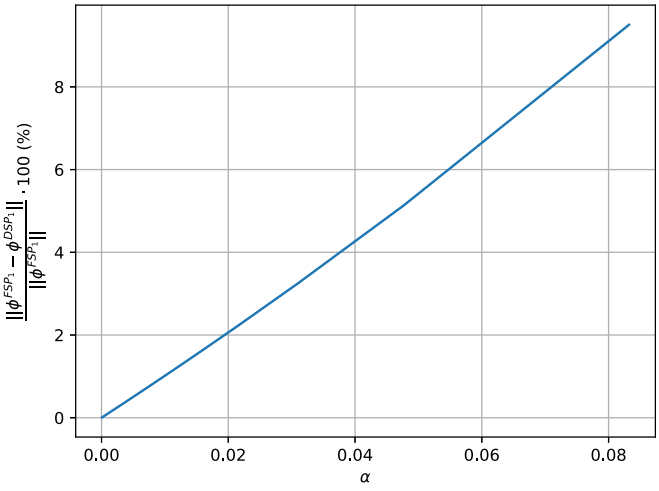

Fig. 1. Relative differences between the FSP_1 and DSP_1 scalar fluxes vs the coefficient α for the homogeneous reactor.

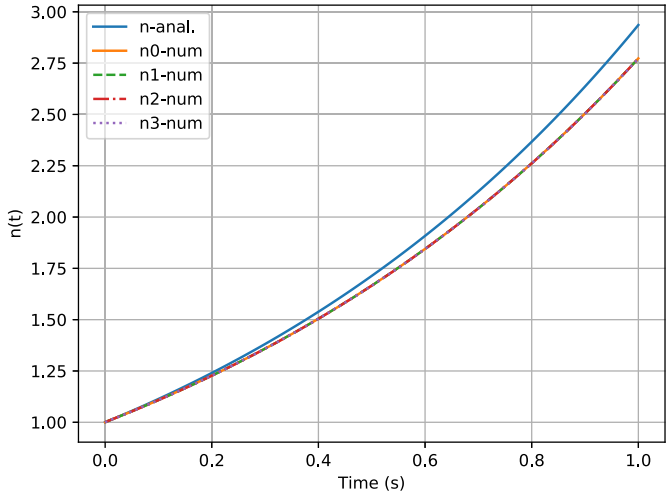

Fig. 2. Analytical and numerical amplitudes $n(t)$ for the FSP_3 equations in the homogeneous problem.

accurate enough results. It must be noted that the errors increase as the transient evolves.

Now, we compare and validate the solutions for the FSP_N and the DSP_N equations ($N = 1, 3$). Table 3 displays the mean relative power (P) computed for the numerical and the analytical solution and the relative local error (LE) at different times. For the numerical approximation, the time-step is set to $\Delta t = 0.001$ s. This Table shows relative local errors between the analytical and numerical solution of 0.1% for the approximations of first order and 0.8% in the approximation of third order. Furthermore, similar values in the numerical relative power between the FSP_1 and FSP_3 are observed. However, if the diffusive and full approximations are compared, differences of $5 \cdot 10^{-2}$ in the power at $t = 1.0$ s can be observed. In this case, the value of α (Equation (71)) is equal to $2.6 \cdot 10^{-2}$ cm^{-1}.

In the following, we test the influence of the value α (Equation (71)) in the difference of FSP_1 and the DSP_1 solutions. For that, different sizes of the slab, L, are taken ($L \in [5, 200]$ cm) to obtain different values of α. The local differences between the scalar fluxes are obtained analytically. Fig. 1 represents the values of α and the differences (in %) at $t = 1.0$ s. The difference increases as the value of α is larger, i.e. lower values of L are chosen. This dependence on the size of the reactor can have implications for the analysis of small reactors such as the small modular reactors (SMR) which are simulated using transport methods that implies the use of supercomputers [24]. In nuclear reactor analysis, usually, the small elements of the reactor are replaced by a homogenized mixture with effective averaged cross sections. In these cases, linear spatial variation of the neutron distribution is satisfied since it appears mean free paths away from the boundary of large (relative to the mean free path) homogeneous media with relatively uniform source distributions. Consequently, diffusion theory is valid and the variation of the odd moments can be then neglected (Stacey, 1969). For more complex analysis, where such small elements are not homogenized, the diffusion fails and the variation of the current must be included in the mathematical model.

Finally, we test the analytical solution of the FSP_3 equations by assuming a point kinetic behaviour. For that, Fig. 2 compares the values of $n_n(t)$ obtained numerically for each moment ϕ^n as

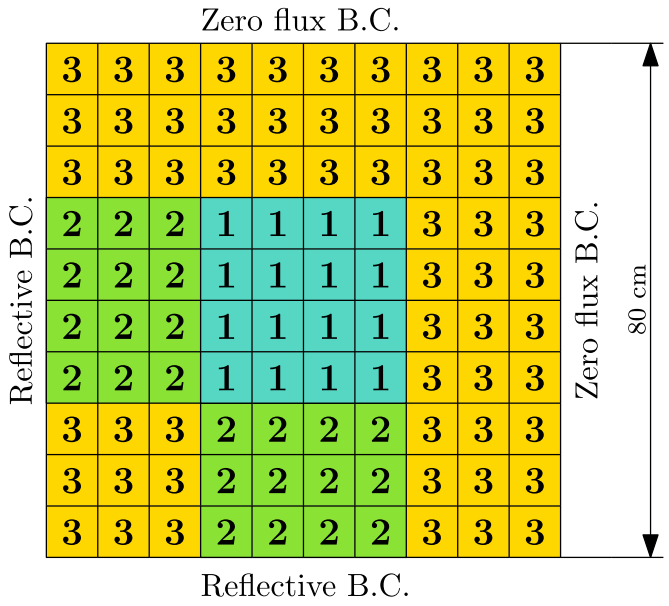

Fig. 3. Geometry and material distribution of the 2D TWIGL reactor.

$$n_n(t) = \frac{\int_\Omega \phi^n(\vec{r},t)dV}{\int_\Omega \phi^n(\vec{r},0)dV}$$

with the analytical $n(t)$ obtained by solving equation (77). This Figure shows that the assumption of the point kinetics approximation (i.e. $n_0 = n_1 = n_2 = n_3$) is an accurate approximation for this problem because in the numerical solution, the numerical amplitudes obtained are overlapped.

6.2. 2D TWIGL benchmark

Two transients for the two-dimensional TWIGL reactor were defined in Ref. [47]. In literature, diffusion codes have provided accurate results for this benchmark. However, there are many other works that provide the solutions by using higher order approximations of the neutron transport. Therefore, the numerical results of this work can be compared with other neutronic codes. In particular, the solution of the SHNC code expounded in Ref. [20] is used. It is a spherical harmonics (P_N) code that uses a nodal collocation method for the spatial discretization. Also, the solution of the diffusion equation from the code QUANDRY is considered. This is equivalent to the DSP_1 solution. This code uses an analytic nodal method [48]. For the spatial discretization, both methodologies have used a mesh of 10 × 10 nodes for the computations.

Table 5
k-effective and problem size (N_t) computed with the FSP_N and DSP_N approximations for the TWIGL reactor. Comparison with the QUANDRY and SHNC codes.

		k_{eff}	N_t
FEMFFUSION	FSP_1	0.913238	5766
FEMFFUSION	DSP_1	0.913234	1922
FEMFFUSION	FSP_3	0.913826	11 532
FEMFFUSION	DSP_3	0.913835	3844
QUANDRY	Diffusion	0.913210	–
SHNC	P_3	0.913753	–

Table 6
Relative power computed with FSP_N and DSP_N approximations ($N = 1, 3$) and comparison with reference methods for TWIGL ramp perturbation.

	FEMFFUSION				QUANDRY	SHNC
	FSP_1	DSP_1	FSP_3	DSP_3	Diffusion	P_3
Time (s)	Relative power					
0.0	1.00000	1.00000	1.00000	1.00000	1.000	1.0000
0.1	1.30874	1.30872	1.31055	1.31051	1.307	1.3115
0.2	1.96053	1.96045	1.96935	1.96920	1.955	1.9746
0.3	2.07544	2.07540	2.08595	2.08583	2.075	2.0900
0.4	2.09281	2.09277	2.10358	2.10345	2.092	2.1075
0.5	2.11032	2.11028	2.12135	2.12122	2.110	2.1252
CPU time (s)	152	28	423	42		

The reactor core is composed of 3 fuel material regions. It is defined for two energy groups and one delayed neutron precursor family. The prompt and delayed spectrum are constant and equal for each material. The values for each energy group are $\chi_1^p = \chi_1^{1,d} = 1$ and $\chi_0^p = \chi_0^{1,d} = 0$. Fig. 3 shows the geometry for a quarter of the reactor, the distribution of the materials and the boundary conditions. Table 4 displays the material cross-section and the delayed precursor data. For the spatial discretization a mesh with 10 × 10 equal cells is considered. The zero boundary conditions are approximated by imposing that $\vec{n}\vec{\phi}^n = 100\ \text{cm}^{-1}\text{s}^{-1}$ for the odd moments in the Marshak's boundary conditions.

Table 5 shows the k-effective obtained with the FSP_N and DSP_N equations ($N = 1, 3$), and the reference values. We do not observe differences between the type of the formulation since the steady-state problem associated is the same. The small differences, of order 10^{-6}, are due to the finite element method approximation. The k_{eff} in the approximations of order $N = 1$ are very close to the diffusion reference result and the k_{eff} in the approximations of order $N = 3$ are closer to the reference for the P_3 approximation. This Table also displays the size of the matrices for each problem, N_t. For this case, the full formulation results in problems which are three times larger than the diffusive formulation.

The full benchmark is composed of two different transients: a ramp and a step perturbation are introduced in the assemblies with material 1, which result in positive reactivity insertions. The time-step for the semi-implicit time schemes selected is $\Delta t = 0.001$ s

Table 4
Cross-section data for the TWIGL reactor.

Mat.	g	Σ_{tg} (cm^{-1})	Σ_{ag} (cm^{-1})	$\nu\Sigma_{fg}$ (cm^{-1})	$\Sigma s_{g,g+1}$ (cm^{-1})	v_g (cm/s)
1 and 2	1	0.238095	0.010	0.007	0.218095	1.0e+07
	2	0.833333	0.150	0.200	0.000000	2.0e+05
3	1	0.256410	0.008	0.003	0.238410	1.0e+07
	2	0.666667	0.050	0.060	0.000000	2.0e+05
$\beta = 0.0065$		$\lambda^d = 0.0065$				

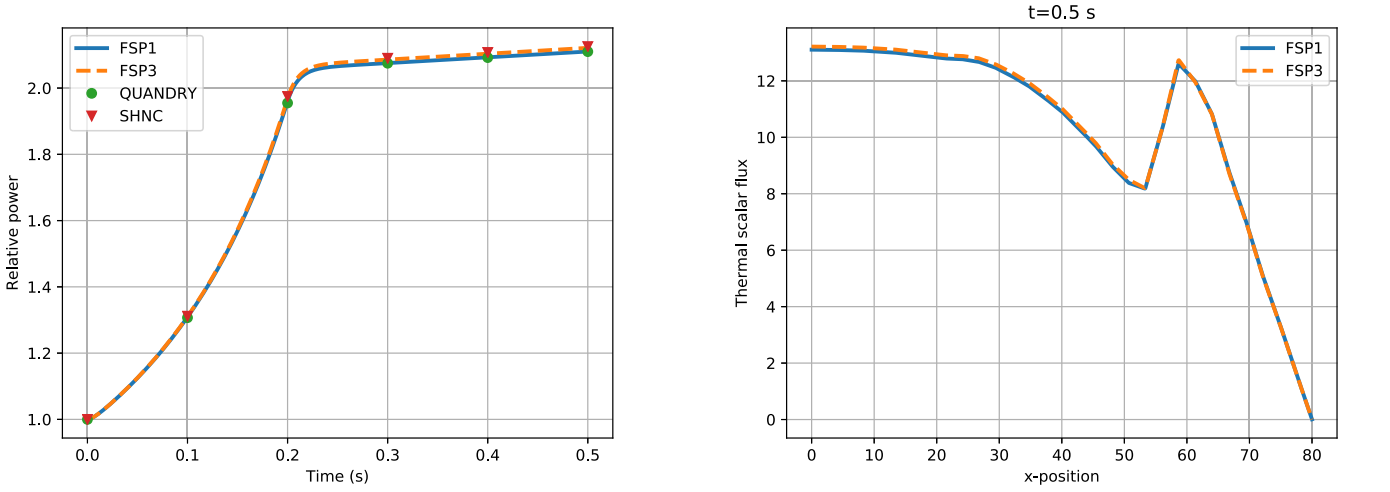

(a) Mean neutron power (b) Thermal scalar flux profile at $y = 40.0$

Fig. 4. Evolution of the mean relative power,P, and thermal scalar flux profile, ϕ_2^0, at $t = 0.5$ for the TWIGL ramp transient.

because we have seen convergent results in the previous case with this value.

6.2.1. Ramp transient

The first transient is defined from a linear ramp perturbation between the times $t = 0.0$ s and $t = 0.2$ s. The absorption cross-section of the material 1 and energy group 2 linearly decrease, from 0.15 cm^{-1} to 0.1465 cm^{-1}. From $t = 0.2$ s the material cross-sections are constant. This can be expressed as

$$\Sigma_{a2}(t) = \begin{cases} 0.15 - 0.11667 \cdot 0.15 \cdot t & 0\ s \leq t \leq 0.2\ s, \\ 0.15 & t > 0.2\ s. \end{cases} \quad (79)$$

The transient is followed during 0.5 s. Table 6 displays the mean relative powers computed with the FSP_N and DSP_N approximations ($N = 1, 3$), and these values provided by the reference codes QUANDRY and SHNC, at different times. The numerical results show a good agreement of FSP_1 and DSP_1 with the QUANDRY results and the solutions of FSP_3 and DSP_3 approximations with the SHNC results in spite of the differences between the approximations of order N = 1 and order N = 3 being from the second decimal place. If the type of time-dependent SP_N formulations are compared, the mean relative power shows differences of 10^{-4} or lower between the full and the diffusive treatments.

In order to compare the computational efficiency of each formulation, Table 6 also includes the computational times (CPU Time) needed to simulate the transient by using the different approximations. The CPU time to simulate the transient with diffusive formulations is much smaller than these values with the full approximations (5 times smaller for $N = 1$ and 10 times smaller for $N = 3$). In fact, it requires less time to simulate the transient with the DSP_3 formulation than if the FSP_1 approximation is used.

Fig. 4(a) represents the evolution of the mean relative power obtained for the FSP_N approximation, the QUANDRY and the SHNC solutions. Fig. 4(b) plots the thermal scalar flux at y = 40 cm and t = 0.5 s for the different approximations. The solutions of the DSP_N equations are no considered because they overlap with the FSP_N curves.

6.2.2. Step transient

The second transient is defined from a step change in the thermal absorption cross-section of material 1. This change can be expressed as

$$\Sigma_{a2}(t) = \begin{cases} 0.15\ \text{cm}^{-1}, & t = 0.0\ \text{s}, \\ 0.1465\ \text{cm}^{-1} & t > 0.0\ \text{s}. \end{cases} \quad (80)$$

Table 7 displays the solutions obtained with FEMFFUSION, QUANDRY and SHNC codes. Fig. 5 shows the mean relative power and the thermal scalar fluxes. As in the previous transient, we observe values in FEMFFUSION results which are very close to the reference results. Moreover, there are no relevant differences between the full and the diffusive approximations for the SP_N equations, but the computational times for the full formulations are very different when they are compared with the diffusive ones, in particular, 5 and 9 times larger.

Comparing with the ramp transient, we observe that for the step transient a prompt increasing of the power is produced whereas the ramp transient produces an increasing with a gentler slope.

6.3. 2D C5G2 MOX benchmark

Finally, two C5G2 MOX transient problems are studied to validate the proposed methodology in a more realistic reactor core. The steady-state C5G2 MOX problem was defined in Ref. [49] as a variant of the C5 MOX fuel assembly problem described in Ref. [50]. This benchmark, in contrast to the previous one, has strong spatial gradients that require higher approximations of the neutron transport equation than the neutron diffusion equation [20]. Hence,

Table 7
Relative power computed with FSP_N and DSP_N approximation ($N = 1, 3$) and comparison with reference methods for TWIGL step perturbation.

	FEMFFUSION				QUANDRY	SHNC
	FSP_1	DSP_1	FSP_3	DSP_3	Diffusion	P_3
Time (s)	Relative power					
0.0	1.00000	1.00000	1.00000	1.00000	1.000	1.0000
0.1	2.06179	2.06175	2.07213	2.07201	2.061	2.0765
0.2	2.07913	2.07910	2.08973	2.08961	2.078	2.0941
0.3	2.09653	2.09649	2.10739	2.10725	2.095	2.1117
0.4	2.11406	2.11402	2.12518	2.12505	2.113	2.1294
0.5	2.13175	2.13171	2.14313	2.14300	2.131	2.1473
CPU time (s)	155	29	383	43		

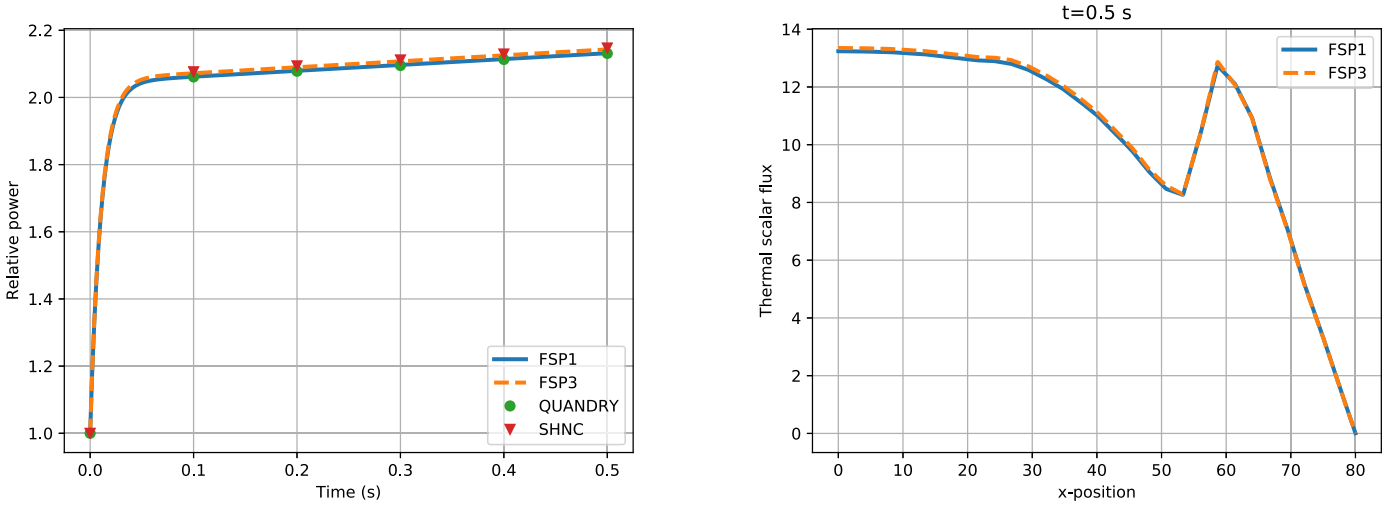

(a) Relative power (b) Thermal scalar flux at $y = 40.0$

Fig. 5. Evolution of the mean relative power, P, and thermal scalar flux, ϕ_2^0, profile at $t = 0.5$ for the TWIGL step transient.

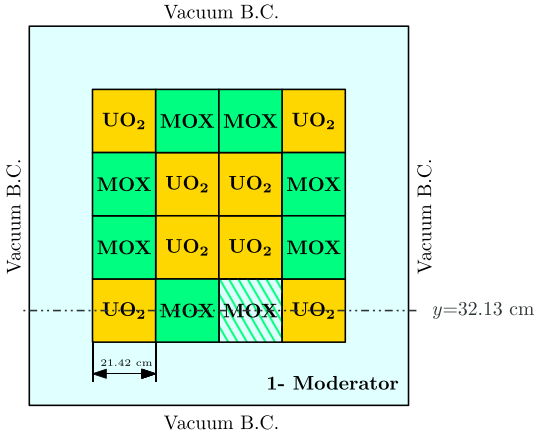

Fig. 6. Geometry and material distribution of the C5G2 MOX reactor.

it will be interesting to use this problem to compare the full and the diffusive formulations of the time-dependent SP_N equations.

Fig. 6 represents the core configuration that is composed of 16 squared fuel assemblies, 8 of type UO_2 and 8 of type MOX. This Figure also shows the size of each assembly and the boundary conditions. Each fuel assembly is in turn divided into 17 × 17 squared pin cells. Fig. 7 shows the configuration for each type of fuel assembly. For the spatial discretization, a square mesh with 84 × 84 cells is considered. Each direction is divided into 8 cells of 2.6775 cm, 68 cells of 1.26 cm and 8 cells of 2.6775 cm. Table 8 contains the homogenized two-group cross-sections for each material. The velocities are generated in Ref. [20] by applying a volume weighting method to collapse the seven energy-group velocities given in the C5G7 benchmark [51] into two energy groups. The data of the eight groups of delayed neutrons are specified in Ref. [51], except the neutron spectra, that are taken as $\chi_1^p = \chi_1^{d,k} = 1$ and $\chi_2^p = \chi_2^{d,k} = 0$.

As reference for the steady-state problem and the Step transient, the solution of the P_3 equations from the SHNC code [44] is used. As reference for these cases, the diffusive SP_1 (Diffusion) and the diffusive SP_3 equations of the PARCS code [52]; [35] are used. In PARCS, the fine mesh finite difference with a mesh of 510 × 510 equal cells is applied.

Table 9 displays the k-effective obtained with the steady-state FSP_N and DSP_N approximations ($N = 1, 3$) and the references. Differences of $2 \cdot 10^{-4}$ in the k-effective are observed between the

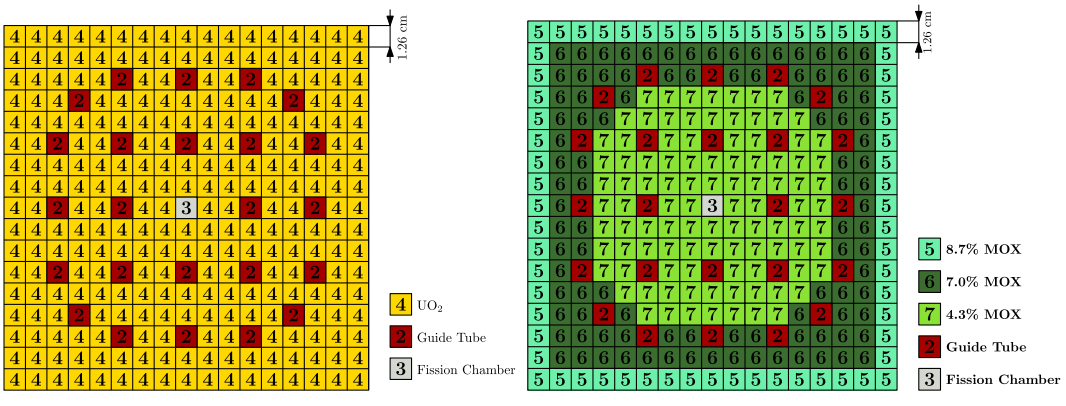

(a) UO_2 assembly (b) MOX assembly

Fig. 7. Geometry and composition of the fuel assemblies for the C5G2 MOX reactor.

Table 8
Cross-section data and velocities for the C5G2 MOX reactor.

Mat.	g	Σ_{tg}	Σ_{ag}	$\nu\Sigma_{fg}$	$\Sigma s_{g,g+1}$	v_g
1 - Reflector	1	0.611	0.001	0.0000	0.050	7.73247e+06
	2	2.340	0.040	0.0000	0.000	2.87886e+05
2 - Guide Tube	1	0.611	0.001	0.0000	0.025	7.68974e+05
	2	2.340	0.020	0.0000	0.000	2.88616e+05
3 - Fission Chamber	1	0.586	0.001	1.0e-7	0.025	8.73088e+05
	2	1.220	0.020	3.0e-7	0.000	2.62899e+05
4 - UO_2	1	0.570	0.010	0.0050	0.020	7.73247e+06
	2	1.100	0.100	0.1250	0.000	2.87886e+05
5–4.3% MOX fuel	1	0.550	0.015	0.0075	0.015	1.22628e+07
	2	1.100	0.200	0.3000	0.000	2.88714e+05
6–7.0% MOX fuel	1	0.550	0.015	0.0075	0.015	1.46202e+07
	2	1.010	0.250	0.3750	0.000	2.92249e+05
7–8.7% MOX fuel	1	0.550	0.015	0.0075	0.015	1.59499e+07
	2	1.060	0.300	0.4500	0.000	2.93512e+05

Table 9
k-effective and problem size (N_t) obtained with the FSP_N and DSP_N approximations for the C5G2 MOX reactor. Comparison with SHNC and PARCS codes.

		k_{eff}	N_t
FEMFFUSION	FSP_1	0.971310	3 84 054
FEMFFUSION	DSP_1	0.971310	1 28 018
FEMFFUSION	FSP_3	0.970792	7 68 108
FEMFFUSION	DSP_3	0.970780	2 56 036
SHNC	P_3	0.970876	–
PARCS	Diffusion	0.971187	–
PARCS	SP_3	0.970542	–

FEMFFUSION and the reference approximations of the same order N. This Table also shows the problem size (N_t) for each case. The difference between the full and the diffusive approximations increases as the problem becomes more complex. In this case, a difference of about $3 \cdot 10^5$ degrees of freedoms appears between the FSP_3 and the DSP_3 problem.

6.3.1. Step transient

The first case studied in C5G2 MOX problem is a Step transient. It is defined by replacing the guide tube material of one MOX assembly (marked in Fig. 6 with a dash pattern) by the reflector material. The transient is followed during 0.05 s. The time-step for the semi-implicit time scheme is set equal to $\Delta t = 10^{-3}$ s.

Table 10 displays the relative power at different time values computed with the FSP_N and DSP_N approximations ($N = 1, 3$) and references [20]. The Table also shows the CPU times needed by the different computations. There are no relevant differences between the diffusive and the full formulations. However, for instance, in the DSP_3 computation, the CPU time is reduced by about 11 times with respect to the FSP_3 computation.

Fig. 8(a) represents the evolution of the mean relative power. This graph shows that the power increases until time $t = 0.04$ s, and then it remains almost constant. Figure shows that the mean relative power value is overestimated by SP_3 approximations in $\approx$6.6% at $t = 0.05$ s in comparison with the P_3 solution. The SP_3 approximations improve the SP_1 results in a $\approx$3.0% when they are compared with the P_3 results.

Fig. 8(b) shows the thermal scalar flux profile normalized in the line $y = 32.13$ cm for the FSP_N approximations at $t = 0.05$ s. This profile is representative of the fuel assembly that has been perturbed. This Figure shows local differences between the approximations of different order N. The solutions of the diffusive approximations are not shown because they are overlapped with the full results.

6.3.2. Noise transient

A second transient studied for the C5G2 MOX problem is a simple neutron noise simulation. A sinusoidal perturbation of 1 Hz is applied to Σ_{a2} of the guide tube material in the MOX assembly marked in Fig. 6 with the dash pattern. The function applied is

$$\Sigma_{a2}^{\text{GT}}(t) = \Sigma_{a2}^{\text{GT}}(0) + 0.1\Sigma_{a2}^{\text{GT}}(0)\sin(2\pi t), \tag{81}$$

The transient is analysed during 3 s.

In this transient, we compare the relative neutron noise defined as

$$\delta\phi^0(\vec{r},t) = \left(\phi^0(\vec{r},t) - \phi(\vec{r},0)\right) \Big/ \phi^0(\vec{r},t), \tag{82}$$

in the frequency domain. For that, the Fast Fourier Transform (FFT) is numerically applied over the time domain results [53]. Only neutron noise results at 1 Hz are shown.

Fig. 9 shows the spatial distribution of the noise amplitude computed with DSP_1 approximation. Similar distributions are obtained with the rest of the approximations. A large influence of the perturbation for the fast scalar flux can be observed. The thermal noise is stronger around the perturbed cells.

First, the approximations of order $N = 1$ are compared. Fig. 10 compares the amplitude of the neutron noise for the fast and thermal groups along the line $y = 32.13$ cm. Fig. 11 provides the comparison for the phase of the neutron noise. These Figures show that the DSP_1 and FSP_1 results are overlapped. The PARCS results are slightly down in the amplitude graphs and slightly above in the phase graphics.

Now, the results for the approximations of order $N = 3$ are compared. Fig. 12 and Fig. 13 compare the amplitude and the phase of the neutron noise along the line $y = 32.13$ cm. In the amplitude

Table 10
Relative power computed with FSP_N and DSP_N approximation ($N = 1, 3$) and comparison with reference methods for C5G2 MOX step perturbation.

	FEMFFUSION				SHNC	PARCS	
	FSP_1	DSP_1	FSP_3	DSP_3	P_3	Diffusion	SP_3
Time (s)	Relative power						
0.000	1.00000	1.00000	1.00000	1.00000	1.00000	1.00000	1.00000
0.001	1.05058	1.05068	1.04655	1.04671	1.04133	1.05651	1.05164
0.002	1.09122	1.09139	1.08381	1.08409	1.07268	1.10116	1.09221
0.005	1.18585	1.18620	1.16993	1.17047	1.14405	1.20199	1.18305
0.010	1.28360	1.28415	1.25773	1.25854	1.21269	1.29713	1.26727
0.020	1.36634	1.36710	1.33041	1.33150	1.26402	1.36611	1.32679
0.050	1.40583	1.40671	1.36380	1.36499	1.28433	1.39197	1.34898
CPU time (h)	1.18	0.44	5.50	0.47			

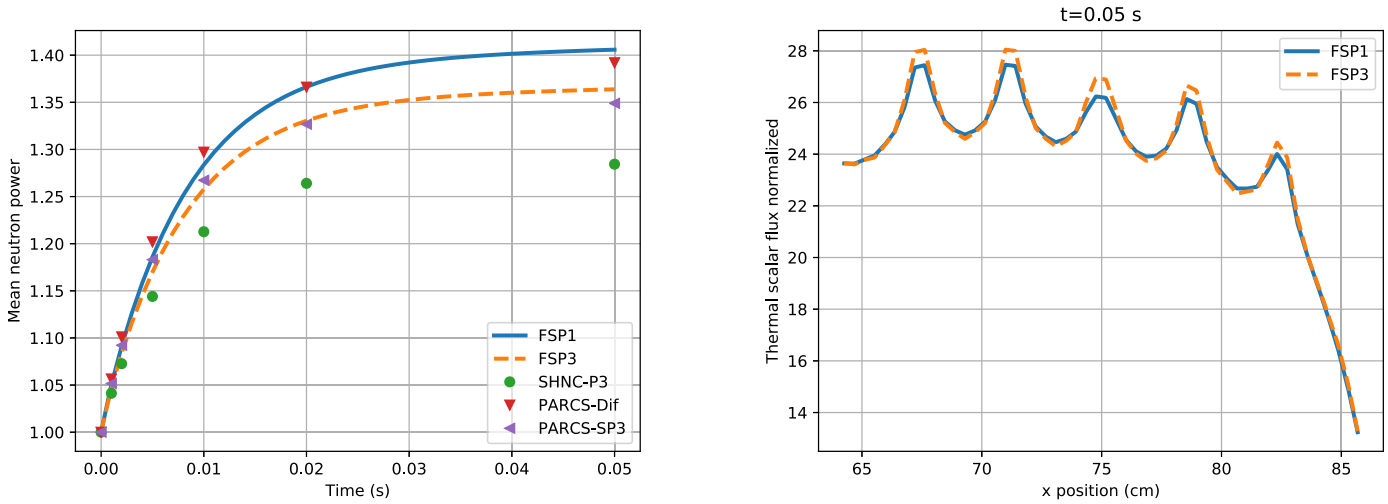

(a) Relative neutron power (b) Thermal scalar flux normalized

Fig. 8. Evolution of the mean relative power, P, and thermal scalar flux profile in the perturbed assembly at $t = 0.05$ s and $y = 32.13$ cm for the C5G2 MOX step transient.

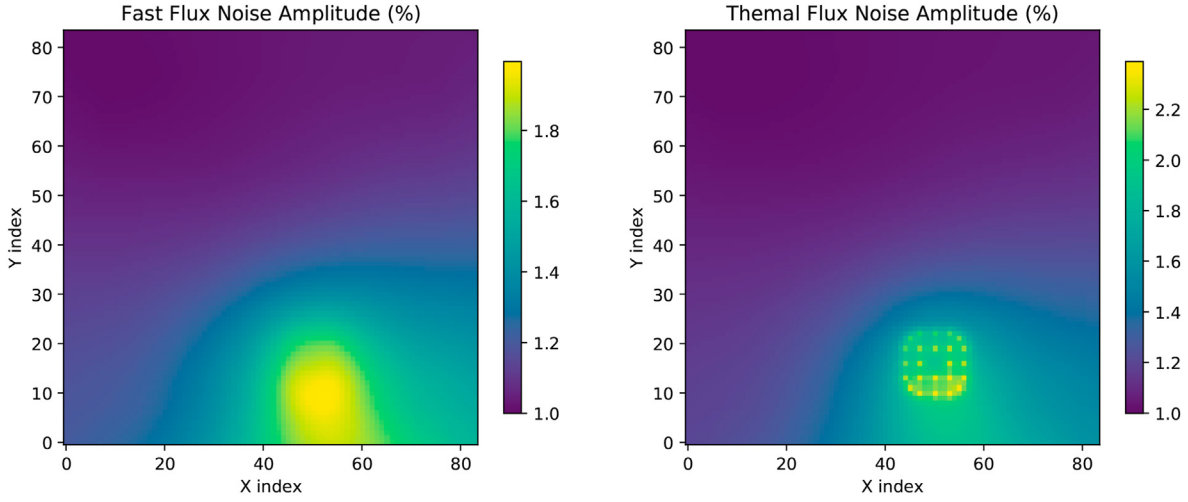

(a) Fast flux noise amplitude (b) Thermal flux noise amplitude

Fig. 9. Noise amplitudes computed with the DSP_1 approximation for the C5G2 noise transient.

graphics, the same conclusions as for the approximations of order $N = 1$ are obtained. However, note that in the phase results, a quantitative irrelevant difference is observed between the full and the diffusive approximations, being the results of the full formulation slightly above from the results of the diffusive formulation ($\approx 0.06^\circ$ at the boundaries of the reactor). In other cases, these differences can be more relevant [33].

7. Conclusions

This paper compares the full formulation for the time-dependent simplified harmonics equations and a diffusive approximation of these equations that neglects the time derivatives of the odd moments obtaining equations with second order derivatives in space, which is a generalization of the neutron diffusion equation. A high order finite element method is used for the spatial discretization of the equations and a semi-implicit time scheme is applied for the implementation of these models in the code `FEMFFUSION`. First, the differences between the time-dependent SP_1 equations are analytically studied for a simple case. Then, the time-dependent SP_1 and SP_3 formulations are numerically studied for more realistic transients. The performance of these methodologies are compared with other transport approximations and neutronic codes as the QUANDRY, the SHNC and the PARCS code.

First, the numerical results show that the time-dependent SP_3 formulations improve the results of the time-dependent SP_1 equations. This improvement is approximately 0.4% in the relative power for the TWIGL reactor and 3% for the C5G2 MOX reactor. It is well known that diffusion approximation does not provide accurate results when strong flux gradients are presented. This happens, for instance, if the reactor consists of many small elements, some of them highly absorbing, as it is the case of the C5G2 MOX reactor.

The numerical results also provide evidence that using the diffusive formulation of the time-dependent SP_N equations is more

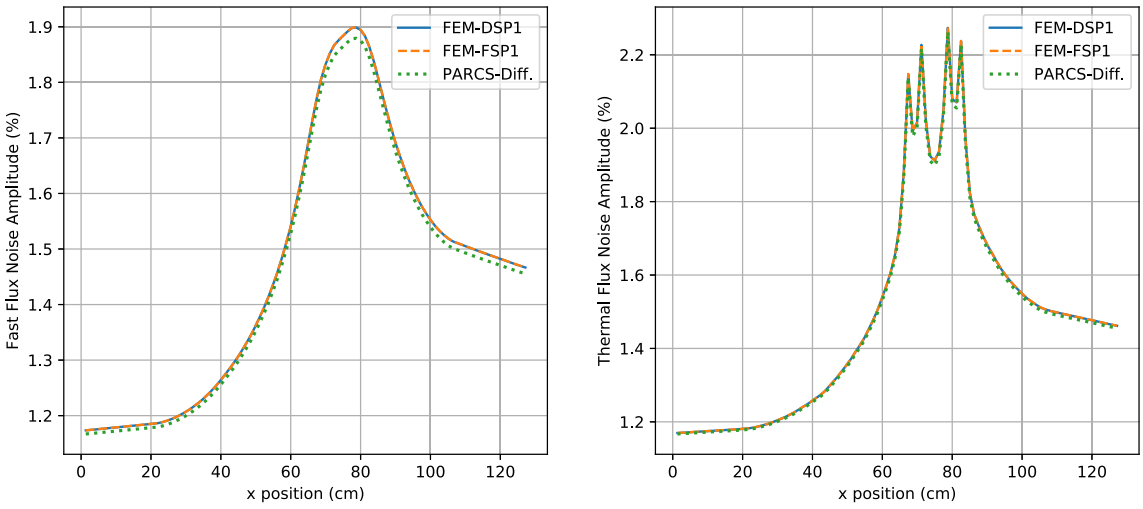

(a) Fast flux noise amplitude (b) Thermal flux noise amplitude

Fig. 10. Noise amplitude comparison between the approximations of order $N = 1$ in $y = 32.13$ cm for the C5G2 noise transient.

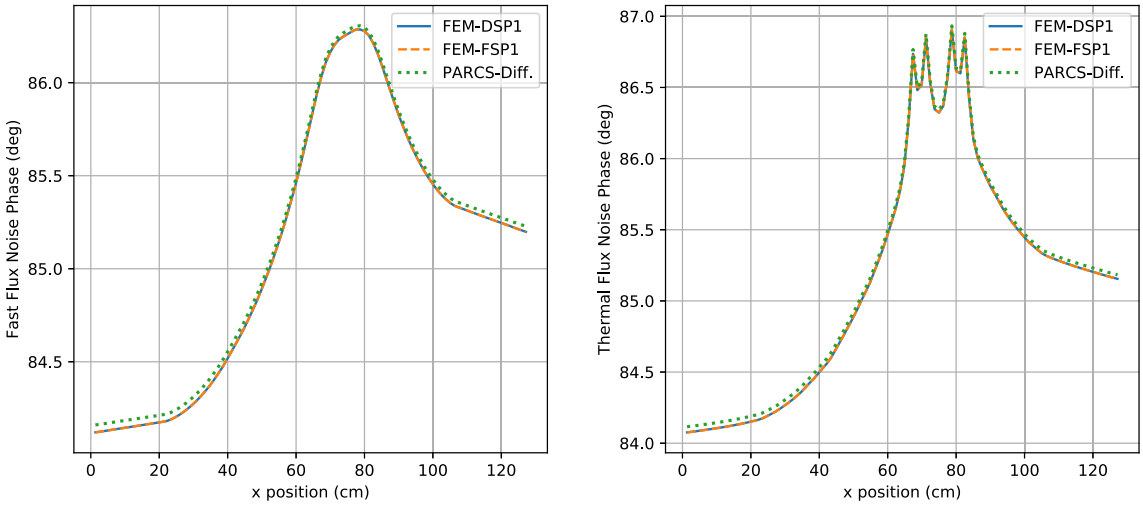

(a) Fast flux noise phase (b) Thermal flux noise phase

Fig. 11. Noise phase comparison between the approximations of order $N = 1$ in $y = 32.13$ cm for the C5G2 noise transient.

efficient than using the full formulation. On the one hand, the analytical solutions of the time-dependent SP_1 equations, for a simple case, show that the differences between the full and the diffusive formulation will mainly depend on the size of the reactor. Only relevant spatial differences, about 0.5%, can be seen in a small reactor of approximately 20 cm, but not longer. This statement is numerically observed for the time-dependent SP_N approximations in more realistic transients. The differences between the relative power with the full and the diffusive SP_3 equations do not reach 0.01% in the transients defined for the TWIGL and C5G2 MOX reactor which have dimensions of 1.6 × 1.6 m and 128.52 × 128.52 m, respectively. On the other hand, if the computational requirements of both formulations are compared, the full formulation of the time-dependent SP_N equations spends more resources than the diffusive formulation to obtain the solution. For a typical problem, the dimension of the matrices obtained from the spatial discretization of the FSP_N equations can be 4 times higher than the matrices obtained with the diffusive formulation. Moreover, the solver for the linear systems needs more time to reach the convergence in the case of the full formulation due to the nature of the matrices involved. In the computational times, these values are between 2 and 11 times higher if the full formulation is used instead of the diffusive formulation.

Therefore, to improve the solution's accuracy in the case of commercial reactors, the authors recommend increasing the number of moments in the time-dependent SP_N approximation and to use the diffusive formulation due to the size of these reactors. The CPU time needed to obtain the solution of the DSP_3 approximation is about 3 times lower than the CPU time if the FSP_1 equations are used, and the accuracy of the DSP_3 solution is significantly higher than the FSP_1 as has been previously pointed out. However, further studies must be performed to confirm this,

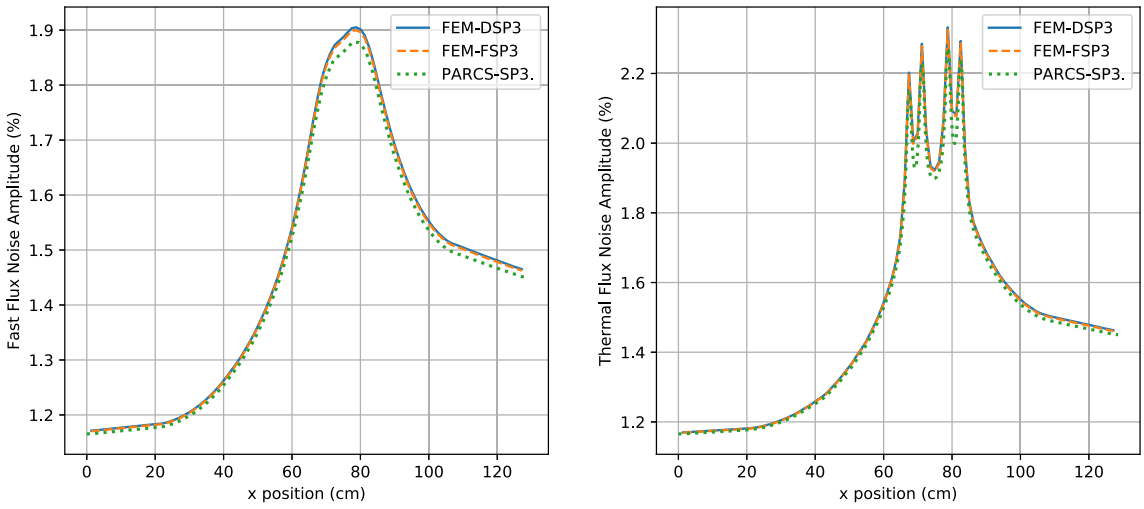

(a) Fast flux noise amplitude (b) Thermal flux noise amplitude

Fig. 12. Noise amplitude comparison between the approximations of order $N = 3$ in $y = 32.13$ cm for the C5G2 noise transient.

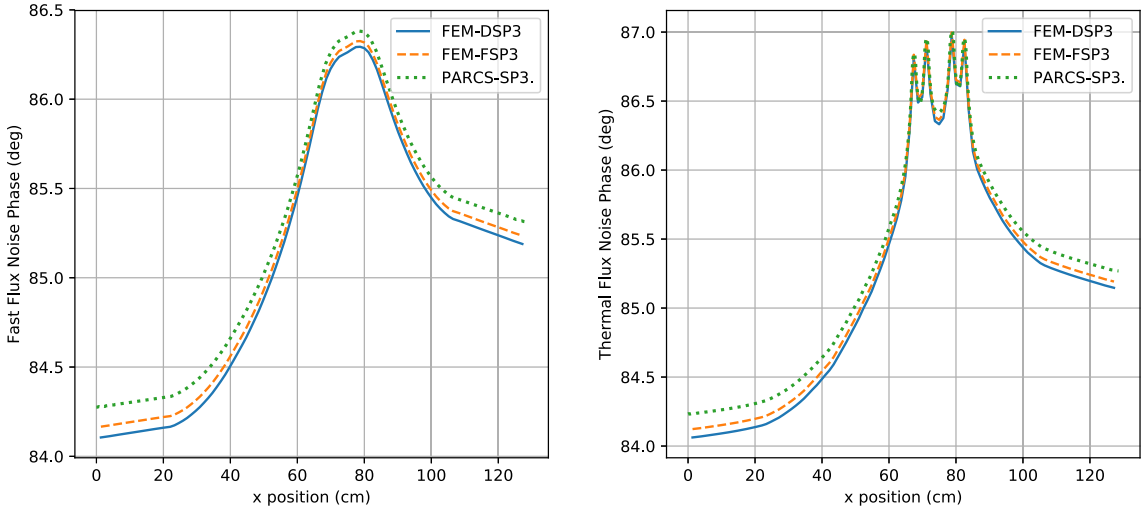

(a) Fast flux noise phase (b) Thermal flux noise phase

Fig. 13. Noise phase comparison between the approximations of order $N = 3$ in $y = 32.13$ cm for the C5G2 noise transient.

especially in small reactors with complex assemblies such as the small modular reactors (SMR).

Declaration of competing interest

The authors declare that they have no known competing financial interests or personal relationships that could have appeared to influence the work reported in this paper.

Acknowledgements

This work has been partially supported by Spanish Ministerio de Economía y Competitividad under projects ENE2017-89029-P and MTM2017-85669-P. Furthermore, this work has been financed by the Generalitat Valenciana under the project PROMETEO/2018/035.

References

[1] W.M. Stacey, Nuclear Reactor Physics, Wiley, Weinheim, Germany, 2007, https://doi.org/10.1002/9783527611041.
[2] B. Sjenitzer, J. Hoogenboom, Dynamic Monte Carlo method for nuclear reactor kinetics calculations, Nucl. Sci. Eng. 175 (2013) 94–107.
[3] N. Shaukat, M. Ryu, H. Shim, Dynamic Monte Carlo transient analysis for the organization for economic co-operation and development nuclear energy agency (OECD/NEA) C5G7-TD benchmark, Nuclear Engineering and Technology 49 (2017) 920–927.
[4] M. Mazaher, A. Salehi, N. Vosoughi, A time dependent Monte Carlo approach for nuclear reactor analysis in a 3D arbitrary geometry, Prog. Nucl. Energy 115 (2019) 80–90.
[5] A. Vidal-Ferràndiz, R. Fayez, D. Ginestar, G. Verdú, Solution of the lambda modes problem of a nuclear power reactor using an *h-p* finite element method, Ann. Nucl. Energy 72 (2014) 338–349.
[6] A. Avvakumov, V. Strizhov, P. Vabishchevich, A. Vasilev, Numerical Modeling of Neutron Transport in SP_3 Approximation by Finite Element Method, 2019 arXiv preprint arXiv:1903.11502.
[7] K. Ivanov, M. Manolova, T. Apostolov, An effective solution scheme of a three-

dimensional reactor core model in hexagonal geometry, Comput. Phys. Commun. 82 (1994) 1–16.
[8] M. Capilla, C. Talavera, D. Ginestar, G. Verdú, Numerical analysis of the 2D C5G7 MOX benchmark using PL equations and a nodal collocation method, Ann. Nucl. Energy 114 (2018) 32–41.
[9] A. Carreño, A. Vidal-Ferràndiz, D. Ginestar, G. Verdú, Spatial modes for the neutron diffusion equation and their computation, Ann. Nucl. Energy 110 (2017) 1010–1022.
[10] W. Stacey, Space-time Nuclear Reactor Kinetics, vol. 5, Academic Press, 1969.
[11] D. Ginestar, G. Verdú, V. Vidal, R. Bru, J. Marín, J. Munoz-Cobo, High order backward discretization of the neutron diffusion equation, Ann. Nucl. Energy 25 (1998) 47–64.
[12] K. Ott, Quasistatic treatment of spatial phenomena in reactor dynamics, Nucl. Sci. Eng. 26 (1966) 563–565.
[13] S. Dulla, E. Mund, P. Ravetto, The quasi-static method revisited, Prog. Nucl. Energy 50 (2008) 908–920.
[14] R. Miró, D. Ginestar, G. Verdú, D. Hennig, A nodal modal method for the neutron diffusion equation. Application to BWR instabilities analysis, Ann. Nucl. Energy 29 (2002) 1171–1194.
[15] A. Carreño, A. Vidal-Ferràndiz, D. Ginestar, G. Verdu, Adaptive Time-step Control for Modal Methods to Integrate the Neutron Diffusion Equation, Nuclear Engineering and Technology, 2020.
[16] B. Ganapol, A more efficient implementation of the discrete-ordinates method for an approximate model of particle transport in a duct, Ann. Nucl. Energy 86 (2015) 13–22.
[17] Y. Chen, B. Zhang, L. Zhang, J. Zheng, Y. Zheng, C. Liu, ARES: a Parallel Discrete Ordinates Transport Code for Radiation Shielding Applications and Reactor Physics Analysis, Science and Technology of Nuclear Installations, 2017. *2017*.
[18] Y. Ma, Y. Wang, J. Yang, ntkFoam: an OpenFOAM based neutron transport kinetics solver for nuclear reactor simulation, Comput. Math. Appl. 81 (2021) 512–531, https://doi.org/10.1016/j.camwa.2019.09.015.
[19] J. Fletcher, A solution of the neutron transport equation using spherical harmonics, J. Phys. Math. Gen. 16 (1983) 2827.
[20] M. Capilla, C. Talavera, D. Ginestar, G. Verdú, Validation of the SHNC time-dependent transport code based on the spherical harmonics method for complex nuclear fuel assemblies, J. Comput. Appl. Math. (2020) 112814.
[21] R. Harel, S. Burov, S. Heizler, The Time-dependent Asymptotic P_N Approximation for the Transport Equation, 2020, p. 1, arXiv preprint arXiv: 2006.11784.
[22] M. Halsall, CACTUS, a Characteristics Solution to the Neutron Transport Equations in Complicated Geometries, Technical Report UKAEA Atomic Energy Establishment, 1980.
[23] J. Yan, B. Kochunas, M. Hursin, T. Downar, Z. Karoutas, E. Baglietto, Coupled computational fluid dynamics and MOC neutronic simulations of Westinghouse PWR fuel assemblies with grid spacers, in: The 14th International Topical Meeting on Nuclear Reactor Thermalhydraulics (NURETH-14), 2011.
[24] F. Alexander, A. Almgren, J. Bell, A. Bhattacharjee, J. Chen, P. Colella, D. Daniel, J. DeSlippe, L. Diachin, E. Draeger, et al., Exascale applications: skin in the game, Philosophical Transactions of the Royal Society A 378 (2020) 20190056.
[25] E. Gelbard, Application of Spherical Harmonics Method to Reactor Problems, Bettis Atomic Power Laboratory, West Mifflin, PA, 1960. Technical Report No. WAPD-BT-20.
[26] G. Pomraning, Asymptotic and variational derivations of the simplified pn equations, Ann. Nucl. Energy 20 (1993) 623–637.
[27] E. Larsen, J. Morel, J. McGhee, Asymptotic derivation of the simplified P_N equations, in: Proceedings of the Joint International Conference on Mathematical Methods and Supercomputing in Nuclear Applications, vol. 1, 1993, p. 718.
[28] R. McClarren, Theoretical aspects of the simplified P_N equations, Transport Theor. Stat. Phys. 39 (2010) 73–109.
[29] E. Larsen, J. Morel, J. McGhee, Asymptotic derivation of the multigroup p_1 and simplified p_n equations with anisotropic scattering, Nucl. Sci. Eng. 123 (1996) 328–342.
[30] A. Klose, E. Larsen, Light transport in biological tissue based on the simplified spherical harmonics equations, J. Comput. Phys. 220 (2006) 441–470.
[31] A. Vidal-Ferràndiz, A. Carreño, D. Ginestar, G. Verdú, A block arnoldi method for the spn equations, Int. J. Comput. Math. 97 (2020b) 341–357.
[32] M. Altahhan, M. Nagy, H. Abou-Gabal, A. Aboanber, Formulation of a point reactor kinetics model based on the neutron telegraph equation, Ann. Nucl. Energy 91 (2016) 176–188.
[33] M. Altahhan, A. Aboanber, H. Abou-Gabal, M.S. Nagy, Response of the point-reactor telegraph kinetics to time varying reactivities, Prog. Nucl. Energy 98 (2017) 109–122.
[34] A. Baudron, J. Lautard, Simplified P_N transport core calculations in the Apollo3 system, in: International Conference on Mathematics and Computational Methods Applied to Nuclear Science and Engineering (M&C 2011). Latin American Section, American Nuclear Society, 2011.
[35] D. Lee, T. Kozlowski, T. Downar, Multi-group SP_3 approximation for simulation of a three-dimensional PWR rod ejection accident, Ann. Nucl. Energy 77 (2015) 94–100.
[36] C. Hauck, R. McClarren, Positive P_N closures, SIAM J. Sci. Comput. 32 (2010) 2603–2626.
[37] S. Hamilton, T. Evans, Efficient solution of the simplified P_N equations, J. Comput. Phys. 284 (2015) 155–170.
[38] O. Zienkiewicz, R. Taylor, P. Nithiarasu, J. Zhu, The Finite Element Method, vol. 3, McGraw-hill, London, 1977.
[39] V. Hernandez, J. Roman, V. V, SLEPc: a scalable and flexible toolkit for the solution of eigenvalue problems, ACM Trans. Math Software 31 (2005) 351–362.
[40] R. Morgan, D. Scott, Generalizations of Davidson's method for computing eigenvalues of sparse symmetric matrices, SIAM J. Sci. Stat. Comput. 7 (1986) 817–825.
[41] S. Balay, S. Abhyankar, M. Adams, J. Brown, P. Brune, K. Buschelman, L. Dalcin, A. Dener, V. Eijkhout, W. Gropp, et al., PETSc Users Manual, Argonne National Laboratory, 2019.
[42] W. Bangerth, R. Hartmann, G. Kanschat, deal.II – a general purpose object oriented finite element library, ACM Trans. Math Software 33 (2007), 24/1–24/27.
[43] D. Ropp, J. Shadid, Stability of operator splitting methods for systems with indefinite operators: Advection–diffusion–reaction systems, J. Comput. Phys. 228 (2009) 3508–3516.
[44] M. Capilla, C. Talavera, D. Ginestar, G. Verdú, A nodal collocation method for the calculation of the lambda modes of the pl equations, Ann. Nucl. Energy 32 (2005) 1825–1853.
[45] G. Niederauer, Neutron Kinetics Based on the Equation of Telegraphy, Ph.D. thesis, Iowa State University, 1967.
[46] A. Vidal-Ferràndiz, A. Carreño, D. Ginestar, G. Verdú, FEMFFUSION: A Finite Element Method Code for the Neutron Diffusion Equation, 2020. https://www.femffusion.imm.upv.es.
[47] L. Hageman, J. Yasinsky, Comparison of alternating-direction time-differencing methods with other implicit methods for the solution of the neutron group-diffusion equations, Nucl. Sci. Eng. 38 (1969) 8–32.
[48] K. Smith, An Analytic Nodal Method for Solving the Two-Group, Multidimensional, Static and Transient Neutron Diffusion Equations, Ph.D. thesis, Massachusetts Institute of Technology, 1979.
[49] M. Capilla, D. Ginestar, G. Verdú, Applications of the multidimensional P_L equations to complex fuel assembly problems, Ann. Nucl. Energy 36 (2009) 1624–1634.
[50] C. Cavarec, J. Perron, D. Verwaerde, J. West, Benchmark Calculations of Power Distribution within Assemblies, Technical Report Nuclear Energy Agency, 1994.
[51] V. Boyarinov, P. Fomichenko, J. Hou, K. Ivanov, A. Aures, W. Zwermann, K. Velkov, Deterministic Time-dependent Neutron Transport Benchmark without Spatial Homogenization (C5G7-TD), Nuclear Energy Agency Organisation for Economic Co-operation and Development (NEA-OECD), Paris, France, 2016.
[52] T. Downar, Y. Xu, T. Kozlowski, D. Carlson, PARCS V2. 7 US NRC Core Neutronics Simulator User Manual, Purdue University, 2006.
[53] A. Vidal-Ferràndiz, A. Carreño, D. Ginestar, C. Demazière, G. Verdú, A time and frequency domain analysis of the effect of vibrating fuel assemblies on the neutron noise, Ann. Nucl. Energy 137 (2020a) 107076.